Nano Research Energy

ISSN 2791-0091 (print); 2790-8119 (online)
https://doi.org/10.26599/NRE.2022.9120037

Review Article

The pursuit of commercial silicon-based microparticle anodes for advanced lithium-ion batteries: A review

Qing Liu, Yunhuan Hu, Xinrun Yu, Yufei Qin, Tao Meng, and Xianluo Hu (✉)

State Key Laboratory of Materials Processing and Die & Mould Technology, School of Materials Science and Engineering, Huazhong University of Science and Technology, Wuhan 430074, China

Received: 30 July 2022 / **Revised:** 6 October 2022 / **Accepted:** 7 October 2022

ABSTRACT

Silicon (Si) is one of the most promising anode materials for high-energy lithium-ion batteries. However, the widespread application of Si-based anodes is inhibited by large volume change, unstable solid electrolyte interphase, and poor electrical conductivity. During the past decade, significant efforts have been made to overcome these major challenges toward industrial applications. This review summarizes the recent development of microscale Si-based electrodes fabricated by Si microparticles or other industrial bulk materials from the perspective of industrialization. First, the challenges for microscale Si anodes are clarified. Second, structural design strategies of stable micro-sized Si materials are discussed. Third, other critical practical metrics, such as robust binder construction and electrolyte design, are also highlighted. Finally, future trends and perspectives on the commercialization of Si-based anodes are provided.

KEYWORDS

silicon, micro-sized particles, lithium-ion batteries, porous structures, polymer binder, electrolyte design

1 Introduction

Lithium-ion batteries (LIBs) have become the dominant power source in our digital and mobile lifestyle since their commercialization by Sony in 1991. However, they have so far failed to relieve people's anxiety about electric vehicles (EVs) due to their high cost, short service life, and especially unsatisfied energy density compared to petrochemicals. However, a universally recognized view is that the traditional lithium insertion chemistry (Rock-chair) based on layered oxide cathodes and graphite anodes has reached the theoretical limit of 350 Wh·kg^{-1} [1–3]. To promise a bright future for the application of LIBs in EVs, more aggressive battery chemistry, such as applying cathodes of oxygen and sulfur and anodes of silicon (Si) and metallic Li, is urgently pursued to achieve energy density up to 500 Wh·kg^{-1} [4–6].

Among various non-carbon anode materials, Si has superior theoretical specific capacity (4,200 mAh·g^{-1}), attractive voltage plateau (0.2–0.4 V vs. Li/Li$^+$), abundant reserves, and low development cost (Fig. 1(a)), thus prompting it to become one of the most promising anode materials for next-generation LIBs [7, 8]. Despite these merits, the progress of replacing graphite with Si in the anode of practical LIBs has seriously lagged. Si has a relatively low electrical conductivity (< 10^{-3} S·cm^{-1}) from the semiconductor nature, resulting in limited rate performance [9–11]. Furthermore, unlike intercalated electrodes, Si as an alloy electrode undergoes a large volume expansion (> 300%) during lithiation. The tremendous volume change causes a large number of compressive and shear stresses. The stress exceeding the bearing limit of Si material would trigger bulk Si particles suffering from surface cracking, fracture, and eventual crushing. As a result, the Si particles will lose electrical contact with the collector, greatly reducing cycle life and losing lithium storage performance [12, 13]. In addition, the large fluctuations in volume tend to deteriorate and thicken the solid electrolyte interphase (SEI). Unstable SEI further exacerbates capacity decay and reversibility deterioration (Fig.1(b)) [14, 15].

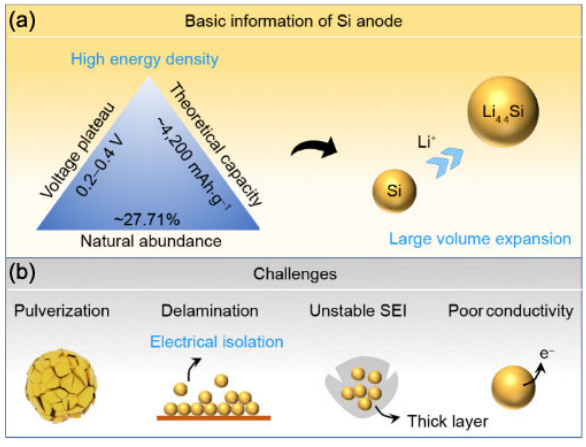

Figure 1 Overview of Si-based anodes for LIBs: (a) merits and (b) fundamental challenges. Reproduced with permission from Ref. [16], © Wiley-VCH GmbH 2021.

Address correspondence to Xianluo Hu, huxl@mail.hust.edu.cn

Many efforts have been made in recent decades to tackle the problems above, such as structure design [17–19], surface modification [20], binder and electrolyte design [21, 22]. The study of Li-Si alloy as anode materials in high-temperature molten salt lithium batteries was first reported in the 1970s [23, 24]. Since then, significant progress has been made in the research on Si anodes (Fig. 2). Among them, nanotechnology has been proven to be one of the effective strategies to buffer the significant volume changes of Si during charging/discharging processes [25, 26]. It was found that Si exhibits greater resistance to mechanical strain and the degree of cracking decreases as the size decreases. 150 nm is determined to be a critical size [27]. Moreover, a wide range of nanoscale materials, including nanowires [28, 29], thin films [30, 31], nanospheres, and nanotubes [13], have been investigated to reduce volume expansion, and a large number of excellent results have also been achieved. Notably, Cui's group has been working on the electrochemical performance and industrialization of Si nanowires in LIBs. In 2007, they first used Si nanowires vertically aligned on the stainless-steel substrate with a diameter of 90 nm as anodes of LIBs [32]. In their study, the improved performance of the LIBs was attributed to the advanced structure of the Si nanowire electrode, which provided enough space between the nanowires to release the strain from large volume changes, and enhanced the electrical contact between the Si nanowires and the substrate. However, scaling up manufacturing, increasing production capacity, and reducing cost remain challenges for its application of EVs.

Apart from the typical electrochemical performances of cycle life and initial Coulombic efficiency (ICE), gravimetric capacity, volumetric capacity, and areal capacity associated with tap density and mass loading are key parameters that must be considered to achieve Si-based anodes for commercial LIBs [33]. Unfortunately, Si nanomaterials have three major drawbacks that hinder their practical application. First, although Si nanomaterials generally accompany with high gravimetric capacity, they display low volumetric capacity due to their inherent low tap density, which is not favorable for space-conscious EVs [34, 35]. Second, the preparation of Si nanomaterials involves a costly and laborious process, which makes their scaling up difficult. Third, using nanoparticles in electrode production may pose serious health and safety risks associated with inhalation or explosion [36]. Recognizing that attractive nano-based performance at the laboratory level is unlikely to be replicated commercially or in practice, current research focuses on microscale Si anodes since it often enables higher tap density and generally higher ICE than nanosized materials.

Many informative reviews have appeared on Si-based anodes during the past decades [37–42]. As to micro-sized Si anodes, Yi et al. highlighted the advances of using nanoscale Si as the building blocks to prepare micro-sized Si anodes [43]. In addition, Zhu et al. also took a comprehensive look at microscale Si-based anodes from the perspective of practical metrics [44]. However, microscale Si-based anodes based on commercial microparticles (MP), such as SiMP, SiO_xMP, Si-metal alloy, and other industrial bulk materials, have not been systematically summarized yet, which is significant for the industrial application in LIBs.

In this review, we are committed to summarizing the development of the Si-based electrodes fabricated by SiMP or commercial Si-based materials from the perspective of industrialization, such as raw materials, preparation process, yield, and environmental friendliness. To begin with, we clarify the challenges for microscale Si anodes. Furthermore, we systematically summarize current strategies of structure design to maintain electrode structural integrity, suppress volume expansion, improve ionic/electronic conductivity, reduce cost, and so on. Furthermore, other critical practical metrics, such as binder and electrolyte, are also discussed. Finally, an outlook on the prospects of future commercialization of Si-based anodes is provided.

2 Challenges for microscale Si anodes

Research on SiMP anodes dates back to the 1900s, predating explosive research on Si nanoparticle (SiNP)-based anodes [45]. However, traditional SiMPs are more likely to suffer from

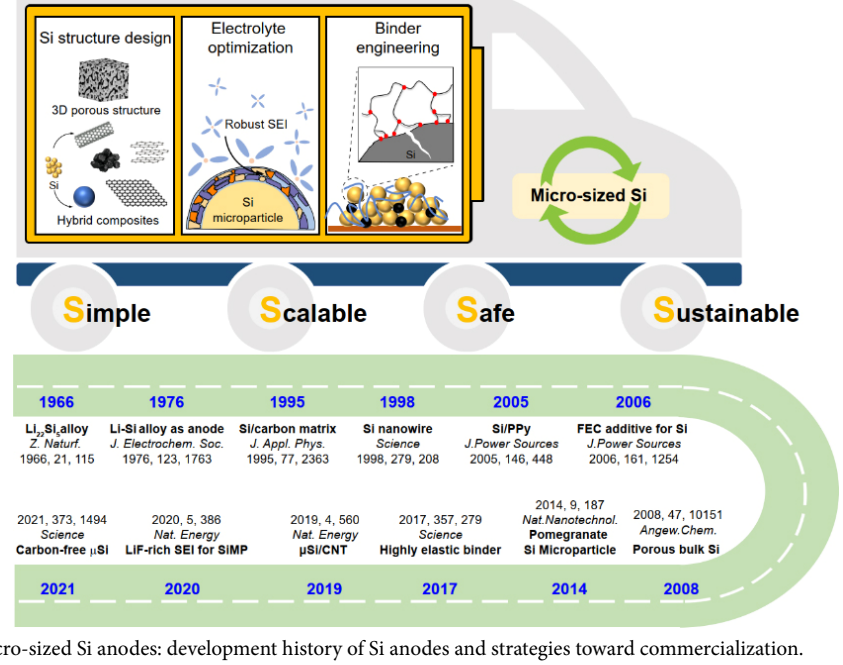

Figure 2 Overview of micro-sized Si anodes: development history of Si anodes and strategies toward commercialization.

severe particle fracture during alloying processes than nanosized materials, leading to rapid capacity decay and battery failure.

Generally, the lithiation of SiMP can be divided into two steps: 1) Li infiltrates the Si lattice at potentials above ~0.1 V (vs. Li^+/Li): the reaction in this process does not involve structural changes or the formation of new phases, in which pure Si is lithiated to amorphous Li_xSi; 2) Lithiated at potentials below ~0.1 V (vs. Li^+/Li): amorphous Li_xSi transforms into crystalline $Li_{15}Si_4$. The corresponding electrochemical reaction are summarized in Eqs. (1)–(4) [46].

Lithiation process ("c" refers to "crystalline" and "a" refers to "amorphous"):

$$\mathrm{Si\ (c)} + x\mathrm{Li^+} + x\mathrm{e^-} \rightarrow \mathrm{Li}_x\mathrm{Si\ (a)} \quad (1)$$

$$\mathrm{Li}_x\mathrm{Si\ (a)} + (3.75 - x)\mathrm{Li^+} + (3.75 - x)\mathrm{e^-} \rightarrow \mathrm{Li}_{15}\mathrm{Si}_4\mathrm{(c)} \quad (2)$$

Delithiation process:

$$\mathrm{Li}_{15}\mathrm{Si}_4\mathrm{(c)} \rightarrow \mathrm{Li}_x\mathrm{Si\ (a)} + y\mathrm{Li^+} + \mathrm{Li}_{15}\mathrm{Si}_4\ \mathrm{(c,\ residual)} \quad (3)$$

$$\mathrm{Li}_x\mathrm{Si\ (a)} \rightarrow \mathrm{Si\ (a)} + x\mathrm{Li^+} + x\mathrm{e^-} \quad (4)$$

Because of electrical disconnection of the active Si caused by a severe volume change, there are some amounts of $Li_{15}Si_4$ phase residual after the initial delithiation (Eqs. (3) and (4)), which results in a large irreversible capacity [47]. Over the complete course of the phase-transition reaction, the two different two-phase regions result in inhomogeneous stress growth, which may lead to capacity fading. Therefore, maintaining the structural stability of Si during cycling is the key to advancing practical application [48].

To address the deficiencies of traditional MP electrodes, engineering the architecture of Si-based materials at the micrometric level to improve the overall performance of Si-based anodes has regained the attention of researchers due to their powerful and comprehensive advantages [49, 50]. To achieve satisfactory electrochemical performances, various microscale hierarchical particles with intriguing nanoachitectures, involving intelligent assembly and nanoparticle-embedded architecture have emerged. However, the strategies using SiNPs as raw materials are not ideal for practical application [51]. In addition, the complex synthesis process of microscale hierarchical particles often involves multiple steps such as chemical vapor deposition, high-temperature treatment, acid treatment, etc., and thus essentially counteracts the low-cost advantages of conventional SiMPs [52–54]. Therefore, it is challenging to construct highly stable SiMP electrodes from the perspective of simple, scalable, safe, and sustainable technology.

3 Rational design of micro-sized Si-based electrode structure

Considerable effort has been devoted to improving the cycling stability of inexpensive Si-based microparticles (SiMP, SiO_xMP, Si-metal alloy, and recycling industrial waste) through various advanced strategies for direct using them as active components in commercial anode materials. These Si-based MP materials have overcome the difficulty faced by Si-based anodes at the nanometric scale and accelerated the commercialization of practical Si-based anode materials. This section is about recent developments in the design of Si-based microparticles through an in-depth discussion in the hope of inspiring future research.

3.1 Scalable synthesis of micro-sized porous Si (μ-porous-Si)

μ-porous-Si and Si-based composites have shown great promise in practical LIBs. On the one hand, the buffer spaces of porous structures can accommodate the volume expansion of Si. On the other hand, the adequate pore structure can provide a large electrolyte-accessible surface area and appropriate space, which shortens a Li-ion transport channel, leading to a better high-rate capability (Fig. 3) [55]. However, scalable synthesis of μ-porous-Si with good cyclability and low cost remains a significant challenge.

In general, bulk materials used as self-template to form porous structure with the combination of the porous structure and interconnected bulk skeleton, shows more commercial feasibility due to the low cost and feasible fabricating procedures. Normally, the methods to fabricate porous Si materials mainly include magnesiothermic reduction [51, 56–58], metal-assisted chemical etching [59–61], template-assisted processes [62], electrochemical etching [63], and dealloying of Si metal alloys [64, 65]. Many studies have reported the preparation of porous Si directly from Si wafers and bulk Si. An attractive study is about the design of a mesoporous sponge Si (MSS) (> 20 μm) with an optimized pore radius based on continuous media mechanical calculation (Fig. 4(a)) [66]. With this unique structure, the as-obtained MSS anode retains more than 80% capacity over 1,000 cycles with high areal capacity (~4.0 $mAh{\cdot}cm^{-2}$) and limited volume expansion (~30%). Subsequently, the porous Si/C electrode prepared by combining MSS with graphite, showed small electrode swelling (< 20%) because of the designed porous structure [67]. Many pore-making processes from Si wafers and bulk Si generally involve high concentrations of HF or HNO_3, which are unfavorable for environmental protection [66, 68–72]. In the current bulk materials, SiO_x has long attracted much attention of researchers [73]. To develop materials combining the advantages of both micro-sized and nano-sized Si materials, Wang's group has conducted a series of studies on the synthesis of micro-sized porous Si/C composites employing commercially available bulk SiO as starting materials. They have developed a facile route to construct the porous structure of interconnected Si and carbon nanoscale building blocks (Fig. 4(b)). Benefiting from the designed structure, the obtained Si/C composite exhibited high reversibility of 97.8% capacity retention after 200 cycles with a high tap density of 0.78 $g{\cdot}cm^{-3}$ [74]. Subsequently, the in-depth investigation revealed that the critical Si building block size is 15 nm, enabling a high capacity without compromising the cycling stability [75]. Furthermore,

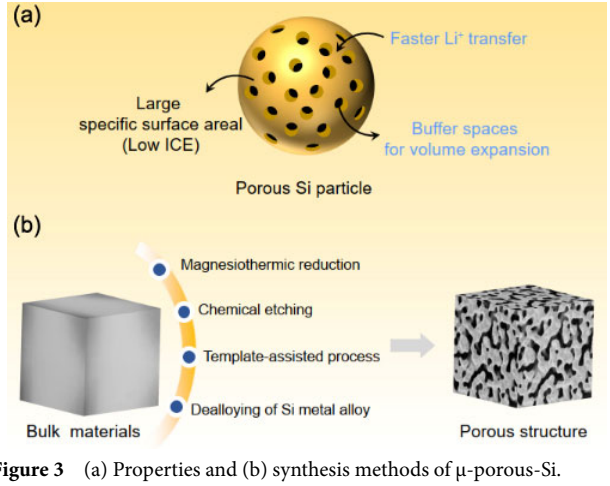

Figure 3 (a) Properties and (b) synthesis methods of μ-porous-Si.

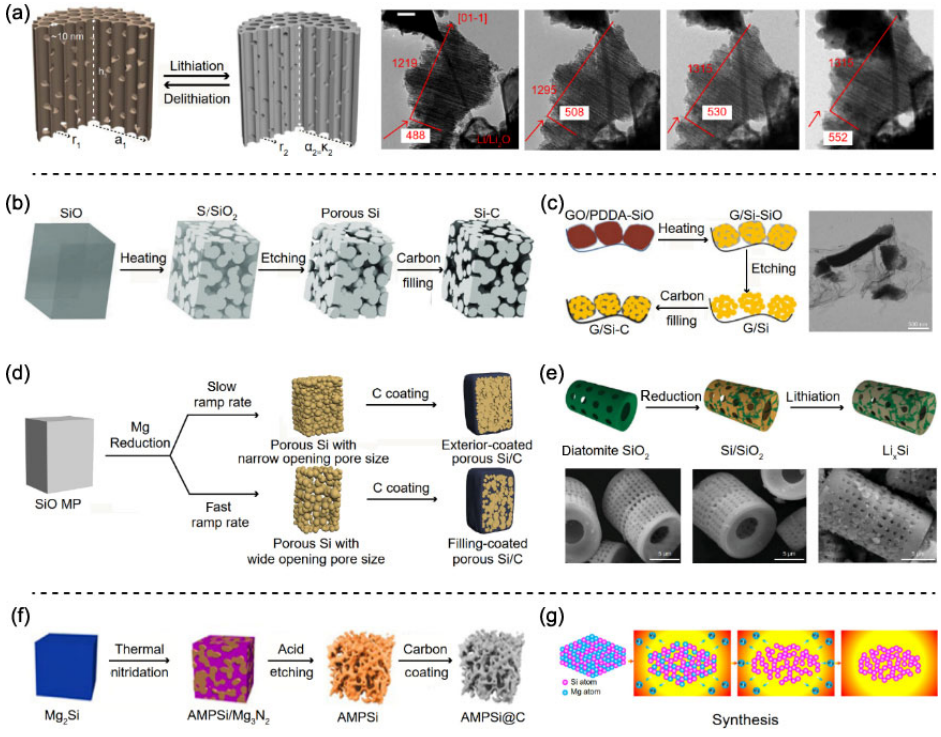

Figure 4 Synthesis of μ-porous-Si. (a) A schematic model of the MSS particle. Reproduced with permission from Ref. [66], © Macmillan Publishers Limited 2014. (b) Preparation process from the SiO precursor to the Si-C composite. Reproduced with permission from Ref. [74], © WILEY-VCH Verlag GmbH & Co. KGaA, Weinheim 2013. (c) Preparation process of G/Si–C. Reproduced with permission from Ref. [76], © WILEY-VCH Verlag GmbH & Co. KGaA, Weinheim 2013. (d) Fabrication of carbon-coated Si/C microparticles. Reproduced with permission from Ref. [77], © Elsevier Ltd. 2017. (e) Schematic illustration of diatomite SiO_2, diatomite-derived Si/SiO_2, lithiated Si, and SEM image of diatomite SiO_2. Reproduced with permission from Ref. [78], © Wiley-VCH GmbH 2020. (f) Schematic showing the preparation of ant-nest-like microscale porous Si (AMPSi) and AMPSi@C. Reproduced with permission from Ref. [79], © An, W. L., et al. 2019. (g) Schematic of the evolution of Mg_2Si alloy by the vacuum distillation method. Reproduced with permission from Ref. [80], © American Chemical Society 2018.

a high areal capacity of 3.2 mAh·cm^{-2} after 100 cycles with high CE was achieved due to dual conductive networks in the presence of graphene (Fig. 4(c)) [76]. Typically, the ICE of μ-porous-Si without a surface coating is far below that of graphite anodes (90%–95%) due to the high specific surface area. Meanwhile, low coating carbon content could increase the first ICE of μ-porous-Si anodes because amorphous carbon irreversibly reacts with lithium at a low potential. Therefore, the coating carbon content needs to be considered comprehensively in the design process. In this regard, exterior carbon coating on μ-porous-Si with pore size of ~2.8 nm was developed, which could significantly reduce specific surface area from 235.6 to 32.4 m^2·g^{-1} [77]. Moreover, the coating carbon content is as low as 5.8 wt.% because the narrow external openings of pores on Si microparticles were easily closed to leave the interior pores unfilled (Fig. 4(d)). Such a design can well-inhibit the irreversible capacity loss, ensuring the high ICE and the integrity of the μ-porous-Si electrode. Impressively, the hierarchically structured μ-porous-Si particles from the low-cost diatomite precursor were realized by one-step magnesiothermic reduction (Fig. 4(e)) [78]. When controlling the reduction time to obtain an optimal ratio between the crystalline Si and the amorphous SiO_2 constituent, the Si/SiO_2 electrode demonstrated a high ICE (~83%) and high capacity retention (90% after 500 cycles at 0.2 C), associated with a low gross cost of ~8.7 $·kg^{-1} in the synthesis process.

The dealloying of Si metal alloys has been demonstrated to provide porous Si materials by removing the element from the original alloys to form the successive 3D porous meshwork structure with interconnected ligaments [55, 81, 82]. Recently, an ant-nest-like bulk porous Si anode was fabricated from bulk Mg_2Si by thermal treatment and acid etching (Fig. 4(f)). Benefiting from the 3D interconnected Si nanoligaments and bicontinuous nanopores, a high areal capacity of 5.1 mAh·cm^{-2} could be achieved at a high mass loading of 2.9 mg·cm^{-2} [79]. Unfortunately, many synthetic methods are still limited to high temperature and mostly involve corrosive HF with low yield, which are not favorable for the feasibility of the practical application [82, 83]. To address this issue, Wang et al. proposed a scalable low-cost HF-free (HCl) approach to preparing μ-porous-Si anodes with a high yield of 90.4% [84]. Although acid-etching has shown attractive potential for the μ-porous-Si anode, the acid solutions in the metal corrosion process still remain a severe environmental issue. In this regard, a green and facile vacuum distillation technique was explored to provide nanoporous Si from commercial Mg_2Si alloy (Fig. 4(g)). The nanoporous Si is formed by the evaporation of low boiling point Mg without pollution. Such a strategy can also secure the pore sizes by adjusting the distillated temperature and time [80]. Subsequently, uniform μ-porous-Si @C was further synthesized by the vacuum distillation method linked with the carbon coating process simultaneously, which is facile and convenient for mass production. By virtue of the catalysis of *in-situ* produced metallic Mg from the Mg_2Si precursor, high graphitization of carbon can be achieved [85]. Recently, Lv et al. designed a large Si cage composite with a Si skeleton and an ultrathin (< 5 nm) mesoporous polypyrrole (PPy) skin. Notably, the practical electrode with ~6.4 mAh·cm^{-2} loading delivered a high specific capacity of ~1,660 mAh·g^{-1} after 400 cycles, showing high potential in mass production of high energy density LIBs [86]. Table 1 summarizes the electrochemical

Table 1 Electrochemical properties of μ-porous-Si electrodes

Anode	Si source	Loading ($mg \cdot cm^{-2}$)	Composition[a]	ICE	Performance		Ref.
					Retention	Cycles	
AMPI@C	Mg_2Si (3–5 μm)	0.8-2.9	80:10:10	80.3%	90.0%	1,000	[79]
NP-Si	Mg_2Si	1.2–1.5	60:20:20	85.0%	59.6%	100	[80]
3D porous Si@C	Si (10 μm)	3.5	75:15:10	94.4%	87.0%	50	[61]
Si_{20}-30 μm	AlSi (30 μm)	0.6	70:15:15	82.0%	83.5%	200	[55]
MBPS/c-PAN	Photovoltaic waste Si (1.5 μm)	1.6	—	92.0%	94.0%	50	[87]
Porous Si/C	SiOMP	1.0	70:15:15	87.5%	75.0%	100	[77]
nC-pSiMP	SiO (325 mesh)	2.0	80:10:10	78.0%	102.0%	1,000	[88]
μ-Si cage	AlSi MPs	4.4	80:10:10	78.2%	86.0%	400	[86]
P-Si/C–1	Metallurgical-grade Si (10-100 μm)	4.2	80:10:10	78.0%	84.0%	50	[68]
3D porous Si	Si-alloy composites	1.0	60:20:20	76.5%	42.0%	200	[81]
Si/C	AlSi alloy (0.5–50 mm)	0.5	60:20:20	81.5%	86.8%	300	[64]
Porous Si	Mg_2Si (3–12 mm)	1.0	80:10:10	84.3%	69.0%	100	[84]
Porous Si/C	SiO (325 mesh)	1.2	60:20:20	77.0%	97.8%	200	[74]
p-Si	Waste crystalline silicon solar panels	0.5–0.9	70:10:20	84.2%	91.5%	400	[89]
Si/SiO_2	Diatomite	1.6	60:20:20	83.0%	90.0%	500	[78]
M-pSi	Si (5–10 μm)	0.5	60:20:20	85.2%	95.0%	100	[72]

[a]Ratio: active material:conductive agent:binder.

performances of recently reported μ-porous-Si electrodes for LIBs.

In brief, as an anode with more practical application prospects due to the long-term cyclability, excellent rate capability, high mass loading, and low electrode swelling ratio, the fundamental challenges in designing μ-porous-Si electrodes are simultaneously attaining cheap, green, and high yields of production processes. Thus, the way to reduce acid consumption and temperature during production and increase the utilization of raw materials is a focus of future research. In addition, the rational distribution of pore structures and balance of the species, content, and uniformity of coated carbon are also noteworthy.

3.2 Si/C composites

SiMPs have been identified as the most promising anodes for cost-effective production. However, it remains a daunting challenge to suppress pulverization effectively and maintain the integrity of SiMP electrodes. Meanwhile, low intrinsic electronic conductivity also limits their rate performance. The rational design of Si/C composites has emerged as an encouraging strategy to overcome these drawbacks. The core of the Si/C composites is to construct strong mechanical support and protection for active SiMP, alleviating mechanical stress from volume expansion, providing rapid transport channels for Li^+ and electrons, and protecting the interface between the SiMP and electrolyte. Various carbon-based materials, such as graphite [90, 91], carbon nanotubes (CNTs)/nanofibles [92], graphene [93], and pyrolysis carbon, were progressively developed to improve the electrochemical performance. For composite SiMP/C anodes, the preparation process should meet high yields and low energy consumption to further achieve large-scale application. Ball milling and spray drying are considered low-cost and effective methods for producing Si-based anodes [52, 94–96]. In this regard, scalable synthesis of Si-graphite microspheres was achieved through a simple two-step mechanical strategy of bead grinding and spray drying (Fig. 5(a)). The few-layered graphite nanosheets play as a buffer layer to alleviate volume expansion and build a conductive framework to enhance electronic conductivity. Owing to the functional structure, the Si-graphite anode delivers a reversible capacity of 1,895 $mAh \cdot g^{-1}$ at 0.5 $A \cdot g^{-1}$ with high-capacity retention of 99.8% over 500 cycles [97].

Graphene, a two-dimensional and flexible carbon material with an ultra-large contact area, can be used to build high-performance hybrid electrodes with a minimized carbon content. In addition, graphene contributes to constructing robust electron/Li^+ transport pathways in Si/graphene composites [93, 98, 99]. To stabilize the non-functional SiMP, Cui group encapsulates Si with a unique graphene cage structure, where the graphene cage acts as a mechanically strong and flexible buffer to confine all the broken Si pieces within. Benefiting from the unique structure, the as-obtained Si@Gr anode delivered an ultra-high ICE of 93.2% in the half cell and outstanding capacity retention (90% 100 cycles) in a full cell [100]. Previous studies reported that carbon encapsulation was hard to simultaneously meet the stringent mechanical requirements during the fabrication and cycling processes. Besides, the loosely porous graphene network is easily deformed and unstable under compression [101–103]. Zhang et al. proposed a scallop-inspired shell engineering strategy to confine high-volume SiMPs for the construction of binder-free and stable anodes (Fig. 5(b)) [104]. The methodology of each SiMP involves an inner overlapped graphene (OG) as a sealed shell and an outer 3D interconnected reduced graphene oxide (RGO) as an open hollow shell. The prepared SiMP@OG@RGO composite could resist high pressure of 3,400 kPa, delivering high volumetric capacity (1,697 $mAh \cdot cm^{-3}$) with a pressing density of 0.46 $g \cdot cm^{-3}$. For withstanding localized high stress generated during the fabrication process and under operating conditions, an imperfection-tolerant unique carbon capsule cellular (3C) architecture was designed [105]. Such a structure, consisting of carbon cages with rational voids interweaved in a cellular dense graphene network (Fig. 5(c)),

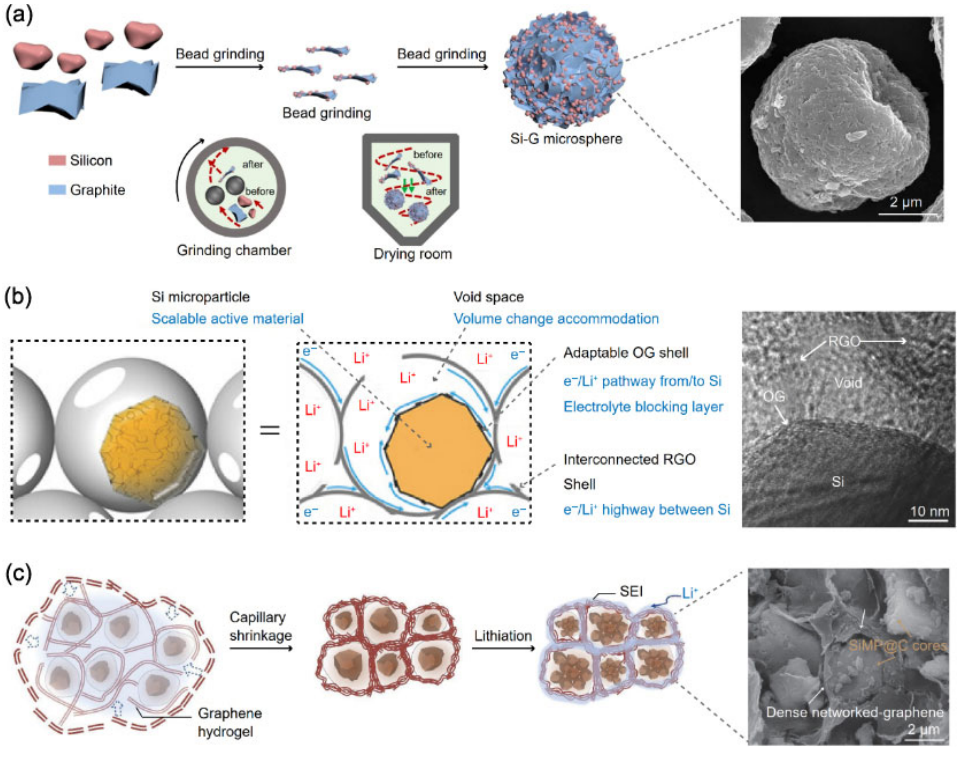

Figure 5 (a) Synthesis diagram of nanostructured Si-G microspheres through a two-step mechanical strategy. Reproduced with permission from Ref. [106], © Wiley-VCH GmbH 2022. (b) Schematic illustration for the structure of mSi@OG@RGO. Reproduced with permission from Ref. [104], © WILEY-VCH Verlag GmbH & Co. KGaA, GmbH 2018. (c) Formation of 3C architecture in SiMP@C-GN. Reproduced with permission from Ref. [105], © Chen, F. Q., et al. 2021.

exhibits 'imperfection-tolerance' to volume variation of irregular SiMPs, achieving a record cyclability over 1,000 cycles. Impressively, an ultrahigh volumetric capacity of 1,048 Wh·L^{-1} was achieved at the pouch full-cell level coupled with a $LiNi_{0.8}Co_{0.1}M_{0.1}O_2$ (NCM811) cathode.

It is demonstrated that the electrical/mechanical properties of electrode materials can be boosted by CNTs, specifically for the shape of segregated networks [107–110]. To overcome the mechanical instabilities of the thick electrodes, a segregated network composite of CNTs with SiMPs was formed by increasing the content of CNTs (Fig. 6(a)) [111]. Such a unique structure allowed the fabrication of high-performance SiMP electrodes with thicknesses of up to 300 μm and enhanced both conductivity and mechanical toughness. The combination of high thickness and specific capacity results in an ultra-high areal capacity of up to 45 mAh·cm^{-2} for the SiMP/CNTs anode in half cells. More practically, the full cells can achieve outstanding areal capacities of 29 mAh·cm^{-2} and specific/volumetric energies of 480 Wh·kg^{-1} and 1,600 Wh·L^{-1}. Recently, Guo group constructed a flexible interface on the surface of carbon-coated SiO_xMPs (SiO_x/C) by infiltrating Li polyacrylate (Li-PAA) with CNTs [112]. The designed interface exhibits regulated stretchability and high electron/Li$^+$ conductivity, maintaining the integrity of the micron-sized C-SiO_x/C electrode and restraining the overgrowth of SEI (Fig. 6(b)). The ingenious design and coating process contribute to the excellent cyclability of the electrode. Besides, Yi et al. reported that CNTs could *in situ* grow into the Si wall and mesoscale porosity to form flexible conductive Si/CNT composites [113]. The unique structure effectively improved the electron transport within the SiMPs, prevented Si domains from pulverization, and enhanced the mechanical properties of SiMP. As a result, the Si/CNT composites delivered a reversible capacity of 715.5 mAh·g^{-1} at 1 A·g^{-1} after 400 cycles. Very recently, a free-standing micro-sized Si-based film anode was reported, whereby the carbon layer and CNT networks doubly anchored the SiMPs through synchronous spraying (Fig. 6(c)) [114]. The networks of Si@CNT@C could catch the Si particles and keep continuous electrical contact during long-term cycling, thus reviving the fragmented Si and maintaining lithium storage properties. The networks fabricated by different types and forms of carbon play a significant role in the electrochemical behavior of Si-based electrodes [53, 115]. It has been of great interest to synthesize Si-based composites with CNTs and graphene [116–118]. A homogeneous and conductive rigid SiMP based gel was successfully prepared by mixing the phytic acid capped Si with graphene oxide and functionalized CNT. The formed 3D cross-linking structure enabled the resultant SiMP-based gel composite with a high reversible capacity of 2,711 mAh·g^{-1} at 0.42 A·g^{-1} and long cycle life of 700 cycles with 800 mAh·g^{-1} [119].

In situ pyrolysis of organic carbon sources is supposed to be an effective method to prepare Si/C electrode materials. Among them, the pitch is an attractive carbon matrix precursor [120, 121], Cho group designed double passivation structured Si/C for high-density composite SiMPs with SiO_2 coated Si and interlayered elastic C derived from pitch [122], such a composite could withstand the induced stress upon repeated cycles, achieving superior cyclability of 1 Ah pouch-type full-cell with a high areal capacity of 3.75 mAh·cm^{-2} and a tap density of 1.65 g·cm^{-3} for 800 cycles. In addition, citric acid [123], polyacrylonitrile (PAN) [124], sucrose [53], phenolic resin [51], etc. could be used for the Si/C composites as carbon precursors.

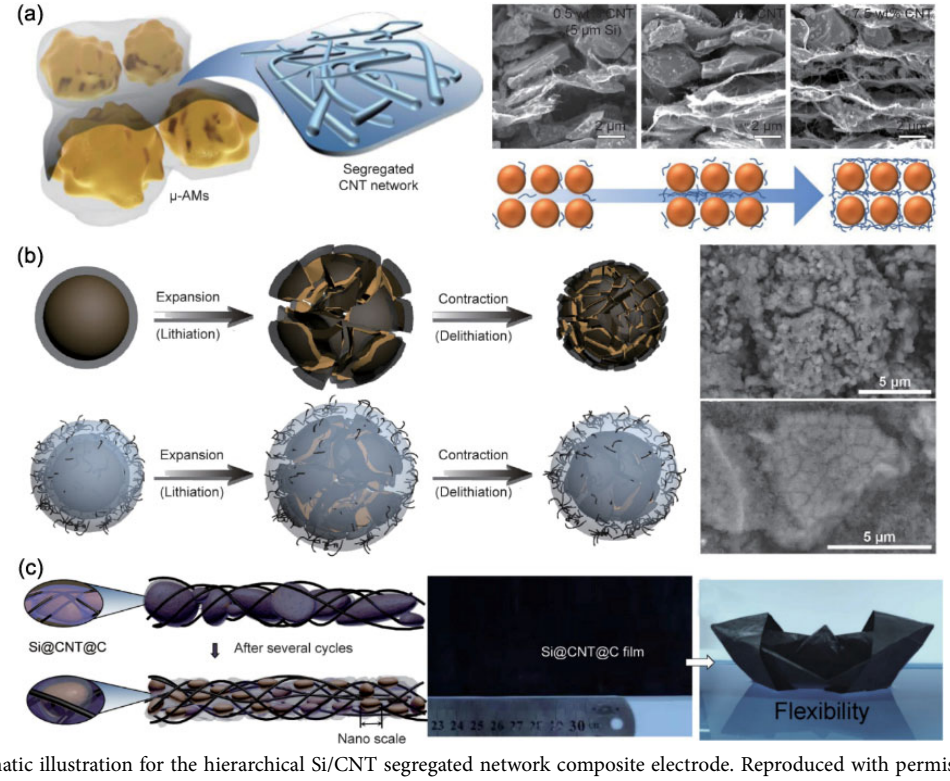

Figure 6 (a) Schematic illustration for the hierarchical Si/CNT segregated network composite electrode. Reproduced with permission from Ref. [111], © Park, S. H. et al. under exclusive licence to Springer Nature Limited 2019. (b) Schematic illustration of the lithiation and delithiation of SiO_x/C and C-SiO_x/C. Reproduced with permission from Ref. [112], © Elsevier Ltd. 2020. (c) Structural characteristics of the Si@CNT@C film. Reproduced with permission from Ref. [114], © Elsevier Ltd. 2021.

In short, the rational design of SiMP/C composites with high electronic conductivity and mechanical strength has greatly improved the cyclability of SiMP electrodes. However, constructing a reasonable multi-scale 3D network to enhance mechanical stability and interface stability for SiMP with different morphologies still needs further investigation. Typically, most synthesis methods of SiMP/C composites are very complex and challenging to scale up (Table 2). Therefore, high yield, environmentally friendly, and economical synthesis methods are urgent.

Table 2 The synthesis methods and electrochemical properties of SiMP/C composites

Anode	Synthesis methods	Loading ($mg \cdot cm^{-2}$)	ICE	Performance		Ref.
				Retention	Cycles	
C-SiO_x/C	Stirring and sonication	1.4–1.5	80.7%	60%	500	[112]
Cross-linked Si/CNT	Acid etching (1 M H_2SO_4) and heat treatment (600 °C)	1.0	60.2%	80.7%	100	[113]
PMSi/CNT/C	Acid etching (2.5 M HF) and heat treatment (800 °C)	1.2–1.5	89.1%	92.6%	50	[110]
Si@CNT@C	CVD, spray, and heat treatment (800 °C)	1.0	74.9%	69.2%	100	[114]
Si/rGO/CNT	Acid etching (HF) and filter	—	82.3%	94%	400	[117]
Si-PA/ GO/CNTs	Ball-milling and self-assembly	0.5–1.5	70.1%	—	—	[119]
Spherical SCG	Ball-milling and heat treatment (1,000 °C)	5.0	84%	99.2%	100	[118]
Si@SiO_2@C	centrifugal mixing and heat treatment (950 °C)	1.1	85.7%	93.2%	50	[122]
SiO_x/SNWs@C	Heat treatment (900 °C–1,100 °C) and CVD	1.8	74.6%	92%	300	[125]
C-MH-2E-SiO_x	Ball-milling, heat treatment (950 °C), and acid etching (HF)	1.0–1.2	78.2%	31.6%	300	[121]
Si/C	Spray-dry and carbonized at 600 °C	1.5	84%	42%	60	[123]
Si/SiO_2@C	Heat treatment (700 °C) and acid etching (1 M HCl)	—	56.8%	70.3%	100	[126]
Porous Si/C–graphite	Acid etching (HF) and CVD	—	63%	82%	450	[67]
MSG	Thermal decomposition (900 °C)	3.0	93%	—	—	[90]
Si-G	Bead grinding and spray drying	0.76	82.4%	99.8%	500	[106]
SiMP@C-GN	CVD and partial etching (NaOH)	1.0	82.6%	70%	500	[105]
Graphene-encapsulatd SiMP	Electroless nickel and carburization, graphene growth at 450 °C, and acid etching (10 M HCl)	0.8–2.5	93.2%	90%	100	[100]
mSi@GNG	Hydrazine vapor reduction	3.0	85%	—	—	[98]
mSi@OG@RGO	Freeze-dried and heat treatment (1,000 °C)	1.0–1.5	78%	—	—	[104]

3.3 The other Si-based composite

In addition to compositing with carbon, Si can also be hybridized with metals [127, 128], metal oxides [129], organic polymers [130], etc., to overcome the application challenges of SiMP [131]. Moreover, recent studies have shown that multicomponent-composited SiMP exhibited improved stability [132]. Inspired by the nanocrystalline 'dispersion strengthening' mechanism of amorphous materials, a novel SiMP composite was developed by a simple and scalable method based on ball milling of prelithiated SiMP in a CO_2 atmosphere, where polycrystalline Si particles embedded in amorphous SiOC matrix contain SiC and Li_2SiO_3 nanocrystals (Fig. 7(a)) [133]. The dispersion-strengthening effect significantly suppressed the volume expansion and particle pulverization. As a result, the prepared DSM-Si anode exhibited a high specific capacity (1,268 mAh·g^{-1} at 100 mA·g^{-1}) and a long lifespan (957 mAh·g^{-1} after 400 cycles) with a tap density of 1.0 g·cm^{-3}. Besides, egg-like few-layered graphene-wrapped and Fe_3O_4-pillared SiO_x anodes (SiO_x@Fe_3O_4@FLG) were synthesized by a highly cost-effective two-step ball-milling technique (Fig. 7(b)). Such a rationally designed mesoporous structure exhibited fast Li^+ diffusion and delivered enhanced cycle stability (500 cycles with 82% capacity retention) [134]. It has proved that highly electron and ion conductive lithiated TiO_2 (Li_xTiO_2, $0 \le x \le 1$) improves electronic conductivity and ion transport kinetics in the bulk electrode related to outstanding rate performance [135, 136]. Inspired by this, dual-shell coating structural composite SiO_x@TiO_2@C was prepared. The as-prepared composite exhibited ultrahigh capacity retention of 89.5% after 800 cycles and excellent rate performance of 949.7 mAh·g^{-1} at 10 A·g^{-1} due to the lithiated TiO_2 with highly ion/electron conductivity [137]. Furthermore, it was also demonstrated that $Li_4Ti_5O_{12}$ (LTO) could enhance the rate performance in an extreme environment. Interestingly, the Si@LTO@C composite displayed a superior reversible capacity of 848 mAh·g^{-1} at an ultra-high current density of 15 A·g^{-1} after 1,000 cycles at 80 °C [138]. Another type of effective coating material is the functional polymer [130]. Lee group combined mechanically resilient coatings of cyclized-polyacrylonitrile (cPAN) with a room-temperature ionic liquid (RTIL) electrolyte to enhance the interface of SiMP and maintain the integrity of electrodes (Fig. 7(c)) [139]. More impressively, incorporating a combustion-reacted nanoporous ZnO matrix into a SiMP electrode (np-ZnO/SiMP) could significantly alleviate volume expansion of Si and stabilize the electrochemical performance (Fig. 7(d)) [140]. The Li_2O/Zn matrix derived from the conversion reaction of np-ZnO acted as an effective buffer to lithiation-induced stresses from volume expansion and served as a binder-like matrix. The np-ZnO/SiMP electrode could achieve a high areal capacity of 1.7 mAh·cm^{-2} beyond 200 cycles with a mass loading of 1.5 mg·cm^{-2}.

4 Binder design for micro-Si anodes

Extensive research has been devoted to developing suitable binders for Si-based anodes.

Although these binders promote the cycling stability of SiNP anodes, achieving long-term durability remains challenging for SiMP anodes because SiMPs are more susceptible to pulverization during volume expansion than their nano-sized particles. Therefore, it is urgent to design binders with satisfactory adhesion and mechanical properties to maintain the integrity of SiMP electrodes.

Severe expansion and cracking phenomenon of SiMP anodes easily lead to the disconnection of the bonding system during Li-cycling processes. Recently, it is demonstrated that the polymer binder with self-healing ability and excellent mechanical properties can restore the losing connection of binder for SiMP systems. Based on the remarkable self-healing and elastomeric properties, Bao and co-workers developed self-healing binders for SiMP anodes with self-healing polymer (SHP). The fabricated SiMP/SHP/CB electrode retained 80% of the initial capacity at 0.4 A·g^{-1} after 90 cycles, which is much higher than that of SiMP electrodes with traditional binders because cracks and damage in the coating during cycling could be healed spontaneously by the randomly branched hydrogen-bonding polymer [141]. To achieve high capacity, long-term cyclability, and rate capability, the same group

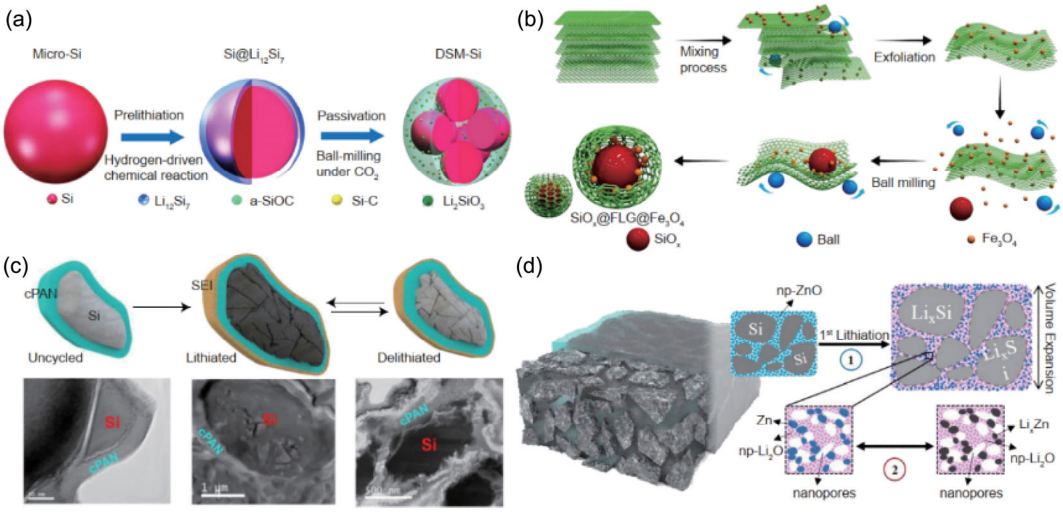

Figure 7 (a) Schematic illustration of the DSM-Si fabrication procedure. Reproduced with permission from Ref. [133], © Elsevier B.V. 2018. (b) Schematic diagram of the two-step ball-milling method for FLG (few-layered graphene)-wrapped and Fe_3O_4-pillared SiO_x composites. Reproduced with permission from Ref. [134], © Elsevier B.V. 2018. (c) Self-contained fragmentation mechanism in which cPAN coatings mechanically confine the fractured μSi particles. Reproduced with permission from Ref. [139], © IOP Publishing 2018. (d) Binder-less, additive-less np-ZnO/SiMP electrode structure and the two-step lithiation mechanism involving the conversion reaction of the np-ZnO and alloying reaction SiMPs that enable extended stable electrochemical cycling. Reproduced with permission from Ref. [140], © American Chemical Society 2018.

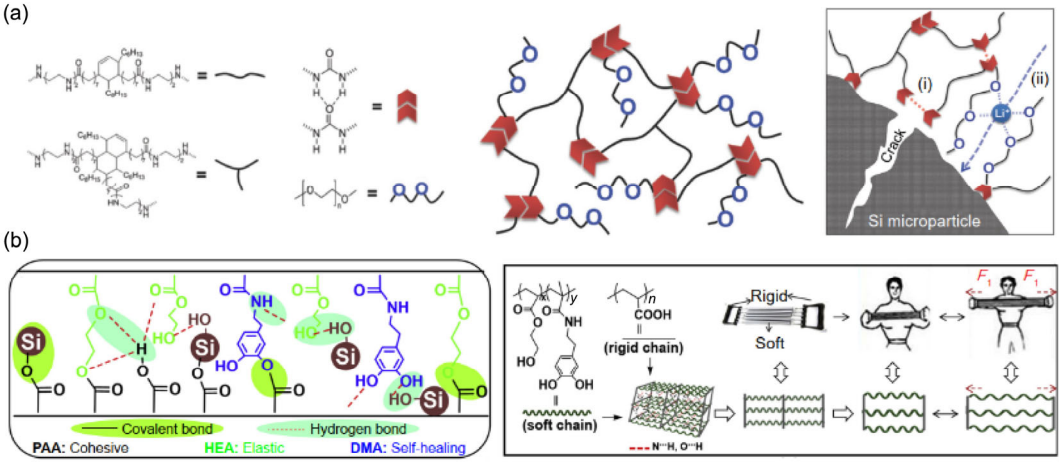

Figure 8 (a) Schematic chemical structure of the SHP-PEG binder and schematic illustration of the Si microparticle electrode with SHP-PEG binder. Left: Self-healing based on dynamic hydrogen bonding close to a crack caused after cycling. Right: Li-ion conduction facilitated by PEG groups. Reproduced with permission from Ref. [142], © WILEY-VCH Verlag GmbH & Co. KGaA, Weinheim 2018. (b) Structural formulae of copolymers and their interaction with Si, chemical structures and illustrative interaction of P(HEA-co-DMA) and PAA. Reproduced with permission from Ref. [143], © Elsevier Inc. 2018.

introduced polyethylene glycol (PEG) groups into the SHP, facilitating Li^+ conductivity within the binder (Fig. 8(a)) [142]. A high discharging capacity of 2,600 mAh·g^{-1} with capacity retention of 80% over 150 cycles at 0.5 C was achieved in the presence of SHP and PEG with M_w 750 in an optimal ratio of 60:40 (mol%). Taking into account the low cost and high safety of the water solvent, Xu et al. designed a water-soluble and rigid-soft modulated polymer binder, poly (acrylic acid)-poly (2-hydroxyethyl acrylate-co-dopamine methacrylate) (PAA-P (HEA-co-DMA), which *in situ* forms a self-healing 3D network flexible structure during the electrode preparation (Fig. 8(b)) [143]. The dual crosslinked network significantly promoted the mechanical strength of the binder, while the soft chains provided good flexibility. The SiMP electrode fabricated with 10 wt.% PAA–P(HEA-co-DMA) binder delivered a high areal capacity of 3.2 mAh·cm^{-2} and capacity retention of 93.8% after 220 cycles at 1 A·g^{-1}, with good rate capability (1,855 mAh·g^{-1} at 5 A·g^{-1}). It is expected that those anode systems hold great promise for practical applications.

Linear poly (acrylic acid) PAA with plentiful carboxyl functional groups that can establish interaction with the Si oxide layer has been extensively investigated in SiNP electrodes. Numerous studies confirm that adjusting softness to improve elasticity, or expanding the network structure of PAA by combining with monomers or polymers, enabled noticeable improvement of application prospects of functional PAA and its derivatives in Si-based systems [144]. Impressively, these strategies have been applied in SiMP anodes with positive results. Choi group designed a novel binder favorable for SiMP anodes by incorporating the sliding-ring polyrotaxane (PR) with PAA. PR altered the mechanical properties of the PAA binder and led to a highly elastic binder network engaging the sliding motion of PR (Fig. 9(a)). Benefiting from the mechanical bond in the form of a PR, the stress generated in the binder during cycling could be uniformly distributed across the networks. Therefore, the PR–PAA binder could accommodate larger stresses without breakage and keeps pulverized particles together without disintegration. Consequently, the fabricated PR-PAA–SiMP electrode (SiMPs, binder, and super P in a weight ratio of 8:1:1) with mass loading of 1.07 mg·cm^{-2} exhibited a high areal capacity of 2.67 mAh·cm^{-2} and attractive capacity retention of 91% after 150 cycles at 0.64 mA·cm^{-2} [145]. Constructing structure-stable SiMP electrodes by linking functional surface coating layer of Si particles and PAA molecular is another effective strategy. A novel method was proposed to synthesize a metal-chelated biomimetic polyelectrolyte coating of Fe^{3+} doped PDA layer on the SiMP surface (Fig. 9(b)) [146]. The subsequent hydrothermal treatment at 160 °C not only generated a Fe–N bond to improve the mechanical strength of the PDA layer, but also formed a 3D crosslinking structure between the PDA layer and PAA to further guarantee the structural stability of anodes (Si@Fe^{3+}–PDA–160/PAA anode). The as-designed electrodes displayed excellent cycling stability with a high capacity retention of 80% after 100 cycles at 0.1 C and stable capacity of 2,000 mAh·g^{-1} after 200 cycles at 0.5 C. In addition, tannic acid (TA) was also used to modify the SiMP and then interact with PAA binder [147]. Under the combined effect of TA and PAA, the formed 3D cross-linked network of binder could improve the cycle and rate performances of low-cost SiMP-based LIB anodes.

Several strategies for improving the mechanical strength of the electrodes and building an extended conductive network have been developed to maintain the conductive network of the Si-based anode. Notably, the conducting binder can perform both electrical connection and binding functions [148]. Nevertheless, the applications of conductive binders are generally hindered by the lack of mechanical strength. To address this issue, Pan and co-workers designed a polyfluorene-type cross-linked conductive binder (CCB) with a robust hierarchical conducting network by connecting linear conductive binders (LCBs) onto conjugated anchor points based on covalent bonds. The synthesized CCB has significant intrinsic conductivity to act as a secondary conductive network and exhibits excellent mechanical properties to maintain the network [149]. Such a robust hierarchical conducting network endows the SiO_x/CCB electrodes with a high capacity retention of 88.1% after 250 cycles at 0.8 A·g^{-1}. Very recently, the same group constructed a water-soluble polyfluorene-type conductive terpolymer (PFPQDA) binder, which consists 10 mol% of dopamine-functionalized fluorene structure units (DA) and 10 mol% of phenanthraquinone PQ groups in the backbone of polyfluorene-typed (PF) conductivity binder (Fig. 10(a)) [150]. The designed triblock

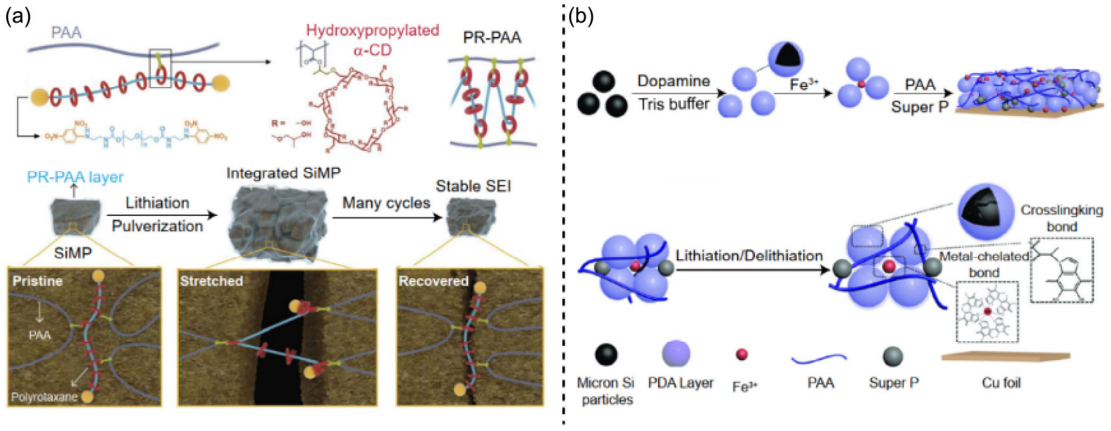

Figure 9 (a) Proposed stress dissipation mechanism of PR-PAA binder for SiMP anodes. Reproduced with permission from Ref. [145], © American Association for the Advancement of Science 2022. (b) Graphical illustrations of the synthesis process of Si@Fe^{3+}–PDA/PAA anode and suppression of Fe^{3+}–PDA/PAA binder on volume expansion of SiMP. Reproduced with permission from Ref. [146], © WILEY-VCH Verlag GmbH & Co. KGaA, Weinheim 2020.

copolymer PFPQDA exhibits enhanced conductivity inherited from PFPQ-COONa (PFPQ) and superior mechanical properties due to the decoration of catechol groups. Consequently, the micro-sized SiO_x anodes with PFPQDA exhibited improved cycling performance (capacity retention of 96% after 150 cycles at 0.1 C) and rate capability with an areal capacity over 2.5 mAh·cm^{-2}, which is attributed to the suppressed volume expansion and stable conductive pathways of electrodes. Besides, it is demonstrated that the n-type conductive polymer binders (CPBs) serve as unique binders for fast-charging SiMP anodes. By introducing a proper amount of 4,4-diphenyl ether and lithium sulfonate groups, aromatic polyoxadiazoles (PODs) can be dissolved in many aprotic polar organic solvents and obtain excellent processability (Fig. 10(b)) [151]. The prepared b-POD CPBs in the eigenstate and n-doping state contained electron-withdrawing oxadiazole ring groups and easily ionizable sulfonate polar groups, enabling excellent ionic conductivity, outstanding wettability to the electrolyte, improved electronic conductivity, and exceptional strength and ductility. Hence, the b-POD endowed SiMP anodes with better cycling performance than non-conductive binders, especially at high current densities.

For improving the mechanical properties of the binder, ensuring the conductive network of electrodes, and enhancing the binding interaction with Cu current collectors, a series of binders with crosslinked networks using various metal cations, supramolecular, and functional polymers or monomers were also developed to overcome the challenges of SiMP electrodes [152–158].

In summary, binders, an indispensable electrode component, play a crucial role in stabilizing Si-based anodes with high volume changes. However, SiMP anodes suffering from more severe fractures during cycling, are compulsory to meet higher requirements on the mechanical properties, interface compatibility, and functionality of the binder. The binder design strategies mentioned in this section have significantly enhanced the cycling stability of SiMP anodes (Table 3). Nevertheless, there

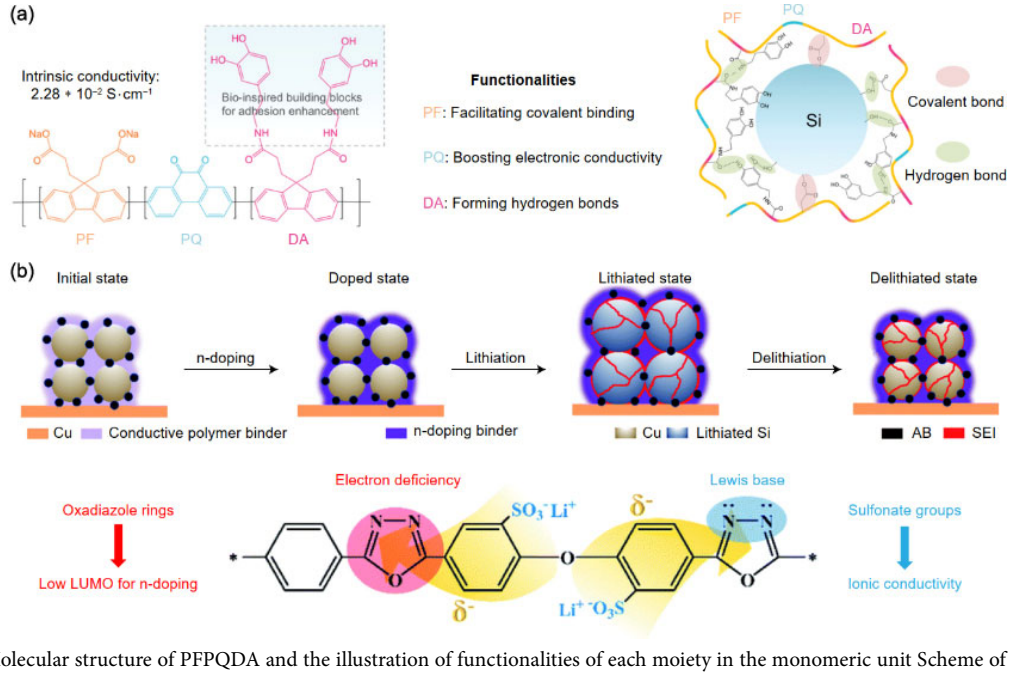

Figure 10 (a) Molecular structure of PFPQDA and the illustration of functionalities of each moiety in the monomeric unit Scheme of multiple networks constructed within Si/PFPQDA electrodes. Reproduced with permission from Ref. [150], © Wiley-VCH GmbH 2022. (b) n-Type CPB that maintains the electrical and mechanical integrity of the SiMP anode during charge and discharge cycles and the chemical structure of aromatic polyoxadiazole lithium sulfonate. Reproduced with permission from Ref. [151], © The Royal Society of Chemistry 2021.

Table 3 Binders for SiMP anodes

Binder	Active materials	Loading ($mg \cdot cm^{-2}$)	Composition[a]	ICE	Performance		Ref.
					Retention	Cycles	
SHP	Si (0.9 μm)	0.7–1.1	70:4:26	—	80.0%	175	[155]
$PANa_{0.8}Fe_y$	Si (1–5 μm)	0.8–1.0	80:10:10	92.3%	64.0%	100	[152]
PFPQDA	SiO_x (6.5 μm)	0.8	80:10:10	72.3%	80.0%	200	[150]
PAL–NaPAA	Si (1 μm)	0.7–0.8	60:20:20	91.0%	—	—	[156]
CCB	SiO_x MP	1.9–2.1	80:10:10	—	88.0%	250	[149]
b-$Li_{0.5}$PAA@SA	Si (1–5 μm)	1.1	60:20:20	86.0%	57.3%	150	[153]
SHPs	Si (3–8 μm)	0.5–0.7	47:6:47	80.0%	80.0%	90	[141]
PR-PAA	Si (1–5 μm)	1.1	80:10:10	91.2%	91.0%	150	[145]
Fe^{3+}–PDA/PAA	Si (1–5 μm)	3.0	60:20:20	—	80.0%	100	[146]
PU-PDA	Si (2–3 μm)	0.3–0.8	60:20:20	71.3%	77.3%	100	[157]
b-POD	Si (0.55 μm)	0.4–0.6	60:20:20	89.0%	—	—	[151]
Li-SPOD	Si (0.5 μm)	—	60:20:20	—	53.4%	100	[148]
PAA-P (HEA-co-DMA)	Si (0.5–1 μm)	0.8–1.0	80:10:10	89.4%	94.0%	220	[143]
TA-PAA	SiMP	0.5	80:10:10	90.0%	61.0%	100	[147]
CMC-co-SN	Si (3 μm)	1.0–1.2	70:15:15	91.5%	—	—	[158]
SHP-PEG	Si (0.8 μm)	0.5–0.7	65:5:30	83.0%	80.0%	150	[142]

[a]Ratio: active material:conductive agent:binder.

are still several challenges in making these binders commercially available, such as complex synthesis processes, expensive raw materials, environmentally unfriendly solvents, low mass loading of active materials, and high proportion of binders. Therefore, more efforts are needed to develop effective binders adapted to the practical applications of SiMP anodes.

5 Design of electrolytes

One of the critical challenges that Si-based materials face is the continual formation of unstable SEI layer, which deteriorates in SiMP anodes due to more severe volume expansion than nano-sized Si particles [159, 160]. Apart from the favorable design and fabrication of Si-based active components and binders, constructing a robust SEI by rational electrolyte design is considered one of the most promising approaches to boost the electrochemical reversibility of Si-based anodes.

Significant progress has been made via functional additives, highly concentrated electrolytes, Li salt, and solvent optimization to further improve the properties of SEI [161–166]. However, the lack of an SEI design principle for alloying anodes inhibits success. The present electrolytes form an organic–inorganic SEI that is strongly bonded to the alloy surface, which makes the SEI suffer from the same high deformation as the alloy. In this regard, Wang's group demonstrated that a rationally designed electrolyte (2.0 M $LiPF_6$ in 1:1 (*v*/*v*) mixture of tetrahydrofuran and 2-methyltetrahydrofuran) facilitates the formation of thin and uniform lithium fluoride (LiF)-based SEIs with a low adhesion (high interfacial energy) to lithiated alloy surfaces [167]. The selective formation of a high-modulus LiF–organic bilayer SEI on the surface of the SiMP electrode enables SiMP to relocate at the interface to accommodate the volume change and maintain particle integrity (Fig. 11(a)). Consequently, SiMP anodes with areal capacities of more than 2.5 $mAh \cdot cm^{-2}$ delivered high ICE of > 90% and average CE of > 99.9% over 300 cycles.

From a practical perspective, high safety under elevated temperatures is necessary for secondary batteries owing to the diversified scenarios and working conditions [168–170]. However, the flammability and volatility of conventional organic electrolytes significantly limit battery operation at high temperatures and cause safety risks. A fire-resistant, well-performing electrolyte and a robust SEI layer derived from the electrolyte are essential to guarantee the safety of Si-based anodes at elevated temperatures [171, 172]. To this end, ionic liquids (ILs) have received intensive attention as alternative solvents to organic carbonates for their remarkable safety features (high thermal stability, nonflammability, and wide electrochemical potential window). Kerr et al. reported that micro-sized Si/graphene anode could deliver outstanding capacity retention of around 3.5 $mAh \cdot cm^{-2}$ after 300 cycles at C/2.5 in an IL electrolyte (trimethylisobutylphosphonium bis(fluorosulfonyl)imide [P1,1,1,i4][FSI] containing a high LiFSI salt content) (Fig. 11(b)) [173]. Moreover, high capacity retention was maintained for 60 cycles at high temperatures up to 80 °C when conventional electrolytes could not operate. The obtained results demonstrated that the highly concentrated IL electrolyte could promote the formation of stable SEI that can accommodate the volume expansion of Si-based anodes.

Elevated temperature generally brings irreversible side reactions and an increased risk of thermal runaway during the operation of a working battery. In general, the decomposition of the commonly used $LiPF_6$/carbonate electrolyte takes place above 55 °C [174], and the SEI starts to disintegrate above 65 °C [175], causing rapid degradation. According to the thermal runaway process of LIBs, the decomposition of SEI is the first step during the occurrence of thermal runaway. When the SiMP anode is employed, the huge volume changes bring more severe challenges of safety at high temperatures. Very recently, Hu's group demonstrated the thermochemical behavior and thermal safety of SEIs on SiMP anodes for high-energy LIBs [176]. The employment of a moderate-concentration IL-based electrolyte, which is compatible with SiMP anodes, is favorable for the formation of robust SEIs with thermally stable, high-modulus, and inorganic-rich features (Fig. 11(c)). Therefore,

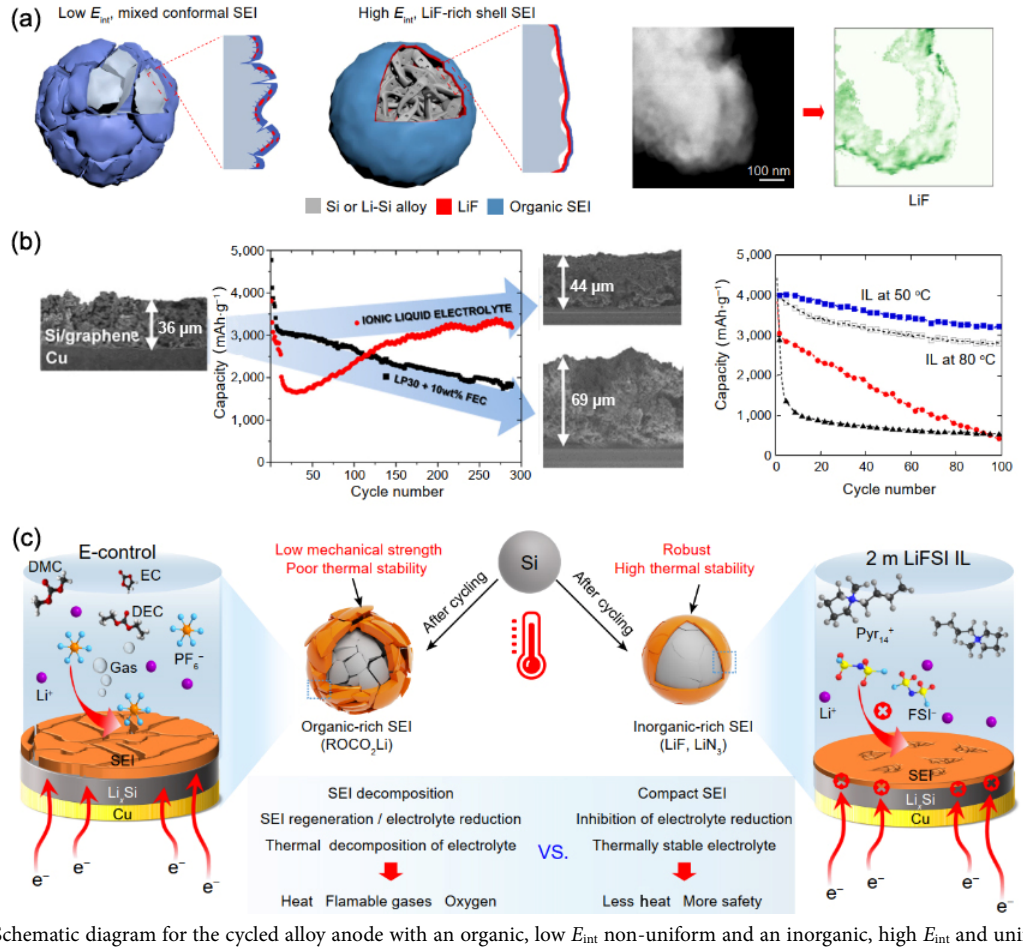

Figure 11 (a) Schematic diagram for the cycled alloy anode with an organic, low E_{int} non-uniform and an inorganic, high E_{int} and uniform Li alloy–SEI interface. Reproduced with permission from Ref. [167], © Chen, J. et al. under exclusive licence to Springer Nature Limited 2020. (b) Comparison of the cycling performance and cross-sectional SEM image of the Si/graphite electrode with and without an ionic liquid electrolyte. Reproduced with permission from Ref. [173], © American Chemical Society 2017. (c) Mechanisms for SEI affecting the battery safety in the E-control electrolyte and IL-based electrolyte at high temperatures. Reproduced with permission from Ref. [176], © Wiley-VCH GmbH 2022.

the thermal runaway would be inhibited by alleviating the decomposition of SEI at high temperatures.

Gel polymer electrolytes (GPE) have been used to improve the safety and stability of batteries [177, 178]. For instance, a supremely elastic GPE was reported to intrinsically alleviating the displacement of material particles and electrode cracking of micro-sized SiO anodes at high loading conditions (Fig. 12(a)) [179]. Attributed to the presence of a soft ether domain and a hard cyclic ring domain, the unique copolymer (poly(poly(tetramethylene-ether) glycol-co-4,4'-methylene diphenyl diisocyanate)-ethylene diamine)) exhibits excellent elasticity, suppressing severe electrode cracking and the peeling-off of SiO particles from the current collector. As a result, a high capacity retention of 70.0% in 350 cycles with a reversible capacity of 3.0 mAh·cm^{-2} and an average CE of 99.9% was achieved when the obtained SiO anode was matched with a $LiNi_{0.5}Co_{0.2}Mn_{0.3}O_2$ cathode. Furthermore, Cho et al. also reported a GPE for the high-loading Si electrode (equivalent to 3.3 mAh·cm^{-2}) with a higher amount of active Si (80%) [180]. The designed GPE provided additional cohesion between the Si particles and retained electrode integrity even after pulverization (Fig. 12(b)). The development of Si anodes for LIBs has been greatly hindered by low interfacial stability against liquid electrolytes. In addition, the amount of inactive components (binders and conductive agents) in the electrodes lowers the energy density of the cells. To address these issues, Meng's group fabricated a battery system with the 99.9 wt.% SiMP anode and sulfide solid electrolytes, enabling the stable operation of the anodes due to the interface passivating properties of sulfide solid electrolytes (Fig. 12(c)) [181]. Bulk and surface characterization demonstrated that this strategy eliminates continuous interfacial growth and irreversible lithium losses. Consequently, SiMP-based full cells could achieve high areal current density, wide an operating temperature range between −20 and 80 °C, and high areal loading of 12 mAh·cm^{-2}.

In brief, maintaining interfacial SEI and electrode structural stability is key to achieving high-performance SiMP anodes. The SEI is predominately determined by the composition of electrolytes (e.g., salt, solvent, and additive) and the chemistry of the electrode surface. Regulating SEI composition and nanostructure by electrolyte design is a straightforward methodology to achieve different properties of interface such as compositional uniformity, enhanced mechanical stiffness, and thermal/chemical stability. In addition, the SEI formation and interfacial evolutions process, as well as the effect of electrolytes on the evolution of electrode structure, should be further understood via operando modes to provide visualized information for the development of functional electrolytes for SiMP electrodes.

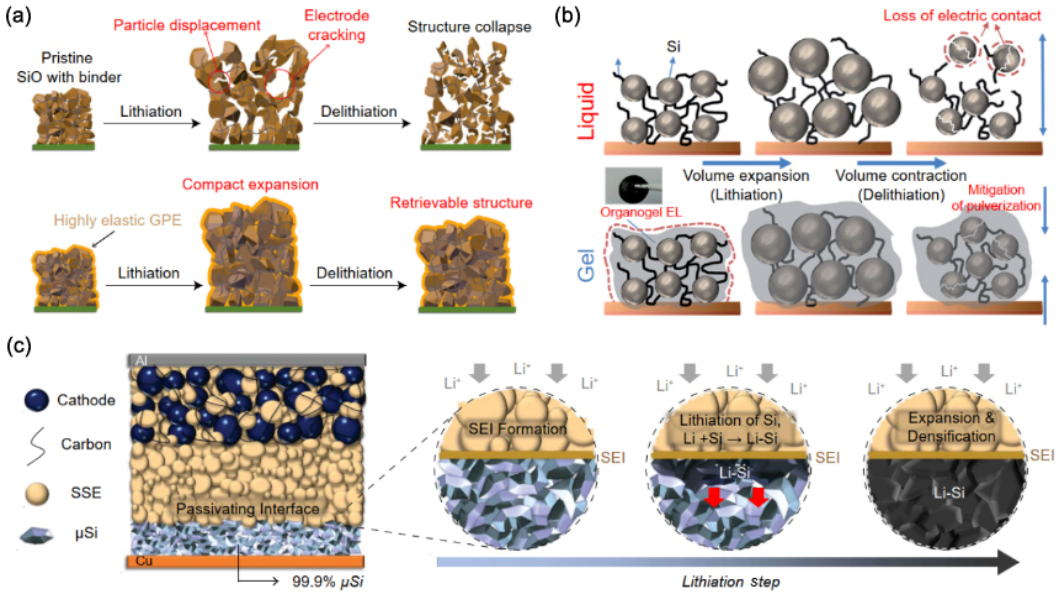

Figure 12 (a) Schematic illustration of an elastic gel polymer electrolyte (GPE)-incorporated SiO anode with a reliable electrode structure. Reproduced with permission from Ref. [179], © Huang, Q. Q. et al. 2019. (b) Morphological changes of silicon electrodes in liquid versus gel electrolytes during lithiation and delithiation. Reproduced with permission from Ref. [180], © The Royal Society of Chemistry 2016. (c) Schematic illustration for the 99.9 wt.% SiMP electrode in an all-solid-state full cell. Reproduced with permission from Ref. [181], © American Association for the Advancement of Science 2022.

6 SiMP-based full cell

Achieving high cyclability of Si-based full cells is even more challenging for Si anode researchers since the capacity fading of Si anodes is more severe in full cells than in half cells. The loss of reversible capacity is not distinct in the half cell, where the Li source is infinitely supplied from the Li metal. In contrast, the consumption of active Li arising from parasitic reactions may result in unavoidable capacity drops in Li-confined full cells [182]. Therefore, investigating the performance in full cells can verify the practical prospect of SiMP-based materials. Table 4 summarizes the performance of SiMP-based full cells.

To satisfy the ever-increasing demands for high energy density, $LiFePO_4$ (LFP) is not a preferential cathode material, despite its stable structure and high safety. The ternary Ni-rich cathode materials and $LiCoO_2$ (LCO) can provide high working voltage and capacity, which have received increasing attention [44].

Pre-lithiation and compatibility are pivotal for SiMP-based full cells with improved energy densities and lifetime [40]. Balancing the structure optimization of SiMP anodes, the design of high-capacity cathodes, the choice of electrolytes, binders, and separators, pre-lithiation technologies, as well as cost reduction remains the urgent challenge of SiMP-based full cells that need to be overcome.

Table 4 Summary of performance for SiMP-based full cells

Anode materials	Cathode materials	Full-cell type	N/P	Energy density ($Wh·kg^{-1}$/ $Wh·L^{-1}$)	Performance		Ref.
					Retention	Cycles	
AMPSi@C	NCM	Coin cell	1.10	502/—	84.0%	400	[79]
P-Si/C@C	NCA	18 650-type cylindrical cell	—	256	84.1%	1200	[56]
Si@C@Al_2O_3	LFP	Coin cell	—	—	70.0%	70	[183]
Si/rGO/CNT	NCM	Coin cell	1.10	—	77.7%	50	[117]
μSi-cPAN	LMR	Coin cell	—	712	85.7%	300	[139]
SiO	NCM523	Coin cell	1.18	—	70.0%	350	[179]
SiMP/GO	LCO	Coin cell	1.00	—/801	—	—	[184]
Si@SiO_2@C	LCO	Pouch cell	1.10	—	—	—	[112]
Porous Si/C	NCM	Coin cell	1.1	—	83%	300	[67]
SiMP@Gr	LCO	Coin cell	1.13	—	90%	100	[100]
Si-G	NCM523	Pouch cell	1.10	—	79.3%	800	[106]
SiO_x	LFP	Pouch cell	1.30	—	—	—	[150]
PR-PAA-SiMP	NCA	Coin cell	1.15	—	98%	50	[145]
μSi	NCM811	Pouch cell	1.10	—	80%	500	[181]
SiMP	NCM	Coin cell	1.10	—	80.8%	120	[143]
Si/CNT	LCO	Coin cell	1.2	—	76%	50	[113]
p-Si	NCM622	Coin cell	—	442/—	75.5%	100	[89]
mSi@OG@RGO	LCO	Coin cell	1.10	—	—	—	[104]

7 Conclusion and perspective

Si is regarded as one of the most promising anode candidates for next-generation LIBs. Solving the challenges caused by severe volume expansion of Si-based electrodes is the prerequisite for commercial application in LIBs. To this end, extensive work has been devoted to promoting the Si-based anode technology. Despite the significant improvement, the large-scale commercialization of Si-based anodes remained a challenge. Firstly, nanotechnology, which enables electrode structural stability and long-term cycling, fails to meet the requirements of industrial applications because of its low tap density, significant side reaction, low volumetric capacity, and complex production process with low yields. Secondly, despite the design of microscale Si-based anodes has remarkably improved the overall performance of the electrode, many production processes still involve elaborate fabrication steps at the cost of energy consumption, environmental pollution, and low yields. Moreover, many microscale Si materials still use nanoparticles as raw materials, which are not favorable for large-scale production. Hence, realizing the application of low-cost manufacturing Si-based materials (SiMP, SiO_xMP, Si-metal alloy, and recycling industrial wastes) in LIBs by a simple and eco-friendly path is meaningful.

From this perspective, we summarize the challenges, current strategies of structure design, binder and electrolyte engineering for bulk Si-based anodes. Finally, an outlook on the prospects of future commercialization of Si-based anodes is listed. Maintaining the electrode structure integrity to ensure stable cycling performance is of paramount importance when using the above low-grade Si-based materials as the Si sources. In this regard, scalable synthesis of porous SiMP and hybrid composites has been studied extensively. However, the failure mechanism analysis of designed micro-sized Si is still lacking from multi-scale and multi-physical fields. It is necessary to develop *in-situ* analysis techniques to clarify the relationship between design strategy and electrode performance, such as the effect of pore distribution on stress dispersion and the evolution of active particle structures, and the effect of composite carbon on electrode surface chemistry and electric field distribution. In addition, more attention should be paid to increasing the areal mass loading of active materials. Furthermore, developing simple, green, efficient, controllable, and energy-saving synthesis technology is pivotal to meeting industrial production requirements.

Binder, as an inactive component of electrodes, plays a crucial role in keeping structural integrity. In terms of improving the mechanical strength of the electrodes and building an extended conductive network, developing a multifunctional polymer binder with self-healing and conducting properties is a promising direction. Moreover, naturally derived polymers have found better success in this role due to their high structural advantages. Therefore, the designed synthesis of multifunctional binders through biomass polymers is well worth studying. As to electrolytes, more attention should be paid to interface regulation by rationally designing the solvent structure.

In the future LIB market, high-energy SiMP-based full cells with long-term performance, high safety, and low cost, have application prospects and needs. More effort should be devoted to addressing the design and compatibility of SiMPs anodes, cathodes, binders, electrolytes, and pre-lithiation technologies. In addition, improving the safe operating temperature of SiMP-based full cells cannot be ignored to cope with heat generation during continuous discharge/charge cycles.

Acknowledgements

This work is supported by the National Natural Science Foundation of China (Nos. 52272206, 51972132, and 52002141), and Program for HUST Academic Frontier Youth Team (2016QYTD04).

Declaration of conflicting interests

The authors declare no conflicting interests regarding the content of this article.

References

[1] Cao, Y. L.; Li, M.; Lu, J.; Liu, J.; Amine, K. Bridging the academic and industrial metrics for next-generation practical batteries. *Nat. Nanotechnol.* **2019**, *14*, 200–207.

[2] Liu, J.; Bao, Z. N.; Cui, Y.; Dufek, E. J.; Goodenough, J. B.; Khalifah, P.; Li, Q. Y.; Liaw, B. Y.; Liu, P.; Manthiram, A. et al. Pathways for practical high-energy long-cycling lithium metal batteries. *Nat. Energy* **2019**, *4*, 180–186.

[3] Liang, Y. R.; Zhao, C. Z.; Yuan, H.; Chen, Y.; Zhang, W. C.; Huang, J. Q.; Yu, D. S.; Liu, Y. L.; Titirici, M. M.; Chueh, Y. L. et al. A review of rechargeable batteries for portable electronic devices. *InfoMat* **2019**, *1*, 6–32.

[4] Xia, C.; Kwok, C. Y.; Nazar, L. F. A high-energy-density lithium-oxygen battery based on a reversible four-electron conversion to lithium oxide. *Science* **2018**, *361*, 777–781

[5] Van Noorden, R. The rechargeable revolution: A better battery. *Nature* **2014**, *507*, 26–28.

[6] Whittingham, M. S. Ultimate limits to intercalation reactions for lithium batteries. *Chem. Rev.* **2014**, *114*, 11414–11443.

[7] Cao, C. T.; Abate, I. I.; Sivonxay, E.; Shyam, B.; Jia, C. J.; Moritz, B.; Devereaux, T. P.; Persson, K. A.; Steinrück, H. G.; Toney, M. F. Solid electrolyte interphase on native oxide-terminated silicon anodes for Li-ion batteries. *Joule* **2019**, *3*, 762–781.

[8] McBrayer, J. D.; Rodrigues, M. T. F.; Schulze, M. C.; Abraham, D. P.; Apblett, C. A.; Bloom, I.; Carroll, G. M.; Colclasure, A. M.; Fang, C.; Harrison, K. L. et al. Calendar aging of silicon-containing batteries. *Nat. Energy* **2021**, *6*, 866–872.

[9] Shimizu, M.; Usui, H.; Matsumoto, K.; Nokami, T.; Itoh, T.; Sakaguchi, H. Effect of cation structure of ionic liquids on anode properties of Si electrodes for LIB. *J. Electrochem. Soc.* **2014**, *161*, A1765–A1771.

[10] Xu, Z. X.; Yang, J.; Li, H. P.; Nuli, Y.; Wang, J. L. Electrolytes for advanced lithium ion batteries using silicon-based anodes. *J. Mater. Chem. A* **2019**, *7*, 9432–9446.

[11] Yamaguchi, K.; Domi, Y.; Usui, H.; Shimizu, M.; Morishita, S.; Yodoya, S.; Sakata, T.; Sakaguchi, H. Effect of film-forming additive in ionic liquid electrolyte on electrochemical performance of Si negative-electrode for LIBs. *J. Electrochem. Soc.* **2019**, *166*, A268–A276.

[12] Zhang, Y. G.; Du, N.; Yang, D. R. Designing superior solid electrolyte interfaces on silicon anodes for high-performance lithium-ion batteries. *Nanoscale* **2019**, *11*, 19086–19104.

[13] Wu, H.; Chan, G.; Choi, J. W.; Ryu, I.; Yao, Y.; McDowell, M. T.; Lee, S. W.; Jackson, A.; Yang, Y.; Hu, L. B. et al. Stable cycling of double-walled silicon nanotube battery anodes through solid-electrolyte interphase control. *Nat. Nanotechnol.* **2012**, *7*, 310–315.

[14] Wang, Q. Y.; Zhu, M.; Chen, G. R.; Dudko, N.; Li, Y.; Liu, H. J.; Shi, L. Y.; Wu, G.; Zhang, D. S. High-performance microsized Si anodes for lithium-ion batteries: Insights into the polymer configuration conversion mechanism. *Adv. Mater.* **2022**, *34*, 2109658.

[15] Choi, N. S.; Yew, K. H.; Lee, K. Y.; Sung, M.; Kim, H.; Kim, S. S. Effect of fluoroethylene carbonate additive on interfacial properties

of silicon thin-film electrode. *J. Power Sources* **2006**, *161*, 1254–1259.
[16] Zhang, C. Z.; Wang, F.; Han, J.; Bai, S.; Tan, J.; Liu, J. S.; Li, F. Challenges and recent progress on silicon-based anode materials for next-generation lithium-ion batteries. *Small Struct.* **2021**, *2*, 2100009.
[17] Zhang, L.; Rajagopalan, R.; Guo, H. P.; Hu, X. L.; Dou, S. X.; Liu, H. K. A green and facile way to prepare granadilla-like silicon-based anode materials for Li-ion batteries. *Adv. Funct. Mater.* **2016**, *26*, 440–446.
[18] Nzabahimana, J.; Guo, S. T.; Hu, X. L. Facile synthesis of Si@void@C nanocomposites from low-cost microsized Si as anode materials for lithium-ion batteries. *Appl. Surf. Sci.* **2019**, *479*, 287–295.
[19] Huang, A. M.; Ma, Y. C.; Peng, J.; Li, L. L.; Chou, S. L.; Ramakrishna, S.; Peng, S. J. Tailoring the structure of silicon-based materials for lithium-ion batteries via electrospinning technology. *eScience* **2021**, *1*, 141–162.
[20] Pan, S. Y.; Han, J. W.; Wang, Y. Q.; Li, Z. S.; Chen, F. Q.; Guo, Y.; Han, Z. S.; Xiao, K. F.; Yu, Z. C.; Yu, M. Y. et al. Integrating SEI into layered conductive polymer coatings for ultrastable silicon anodes. *Adv. Mater.* **2022**, 2203617.
[21] Guo, S. T.; Li, H.; Li, Y. Q.; Han, Y.; Chen, K. B.; Xu, G. Z.; Zhu, Y. J.; Hu, X. L. SiO_2-enhanced structural stability and strong adhesion with a new binder of Konjac glucomannan enables stable cycling of silicon anodes for lithium-ion batteries. *Adv. Energy Mater.* **2018**, *8*, 1800434.
[22] Jin, Y.; Zhu, B.; Lu, Z. D.; Liu, N.; Zhu, J. Challenges and recent progress in the development of Si anodes for lithium-ion battery. *Adv. Energy Mater.* **2017**, *7*, 1700715.
[23] Seefurth, R. N.; Sharma, R. A. Investigation of lithium utilization from a lithium-silicon electrode. *J. Electrochem. Soc.* **1977**, *124*, 1207–1214.
[24] Sharma, R. A.; Seefurth, R. N. Thermodynamic properties of the lithium-silicon system. *J. Electrochem. Soc.* **1976**, *123*, 1763–1768.
[25] Yu, Q.; Ge, P. P.; Liu, Z. H.; Xu, M.; Zhou, L.; Zhao, D. Y.; Mai, L. Q. Ultrafine SiO_x/C nanospheres and their pomegranate-like assemblies for high performance lithium storage. *J. Mater. Chem. A* **2018**, *6*, 14903.
[26] Ma, T. Y.; Yu, X. N.; Cheng, X. L.; Li, H. Y.; Zhu, W. T.; Qiu, X. P. Confined solid electrolyte interphase growth space with solid polymer electrolyte in hollow structured silicon anode for Li-ion batteries. *ACS Appl. Mater. Interfaces* **2017**, *9*, 13247–13254.
[27] Chen, X.; Li, H. X.; Yan, Z. H.; Cheng, F. Y.; Chen, J. Structure design and mechanism analysis of silicon anode for lithium-ion batteries. *Sci. China Mater.* **2019**, *62*, 1515–1536.
[28] Pereira-Nabais, C.; Światowska, J.; Chagnes, A.; Gohier, A.; Zanna, S.; Seyeux, A.; Tran-Van, P.; Cojocaru, C. S.; Cassir, M.; Marcus, P. Insight into the solid electrolyte interphase on Si nanowires in lithium-ion battery: Chemical and morphological modifications upon cycling. *J. Phys. Chem. C* **2014**, *118*, 2919–2928.
[29] Kim, G. T.; Kennedy, T.; Brandon, M.; Geaney, H.; Ryan, K. M.; Passerini, S.; Appetecchi, G. B. Behavior of germanium and silicon nanowire anodes with ionic liquid electrolytes. *ACS Nano* **2017**, *11*, 5933–5943.
[30] Shimizu, M.; Usui, H.; Suzumura, T.; Sakaguchi, H. Analysis of the deterioration mechanism of Si electrode as a Li-ion battery anode using Raman microspectroscopy. *J. Phys. Chem. C* **2015**, *119*, 2975–2982.
[31] Usui, H.; Shimizu, M.; Sakaguchi, H. Applicability of ionic liquid electrolytes to $LaSi_2$/Si composite thick-film anodes in Li-ion battery. *J. Power Sources* **2013**, *235*, 29–35.
[32] Chan, C. K.; Peng, H. L.; Liu, G.; McIlwrath, K.; Zhang, X. F.; Huggins, R. A.; Cui, Y. High-performance lithium battery anodes using silicon nanowires. *Nat. Nanotechnol.* **2008**, *3*, 31–35.
[33] Hou, G. L.; Cheng, B. L.; Cao, Y. B.; Yao, M. S.; Li, B. Q.; Zhang, C.; Weng, Q. H.; Wang, X.; Bando, Y.; Golberg, D. et al. Scalable production of 3D plum-pudding-like Si/C spheres: Towards practical application in Li-ion batteries. *Nano Energy* **2016**, *24*, 111–120.
[34] Su, L. W.; Jing, Y.; Zhou, Z. Li ion battery materials with core-shell nanostructures. *Nanoscale* **2011**, *3*, 3967–3983.
[35] Xu, Q.; Li, J. Y.; Yin, Y. X.; Kong, Y. M.; Guo, Y. G.; Wan, L. J. Nano/micro-structured Si/C anodes with high initial Coulombic efficiency in Li-ion batteries. *Chem. Asian J.* **2016**, *11*, 1205–1209.
[36] Hahn, A.; Fuhlrott, J.; Loos, A.; Barcikowski, S. Cytotoxicity and ion release of alloy nanoparticles. *J Nanopart. Res.* **2012**, *14*, 686.
[37] Chen, Z.; Zhang, H. R.; Dong, T. T.; Mu, P. Z.; Rong, X. C.; Li, Z. T. Uncovering the chemistry of cross-linked polymer binders via chemical bonds for silicon-based electrodes. *ACS Appl. Mater. Interfaces* **2020**, *12*, 47164–47180.
[38] Du, A. M.; Li, H.; Chen, X. W.; Han, Y. Y.; Zhu, Z. P.; Chu, C. C. Recent research progress of silicon-based anode materials for lithium-ion batteries. *ChemistrySelect* **2022**, *7*, e202201269.
[39] Ge, M. Z.; Cao, C. Y.; Biesold, G. M.; Sewell, C. D.; Hao, S. M.; Huang, J. Y.; Zhang, W.; Lai, Y. K.; Lin, Z. Q. Recent advances in silicon-based electrodes: From fundamental research toward practical applications. *Adv. Mater.* **2021**, *33*, 2004577.
[40] Guo, J. P.; Dong, D. Q.; Wang, J.; Liu, D.; Yu, X. Q.; Zheng, Y.; Wen, Z. R.; Lei, W.; Deng, Y. H.; Wang, J. et al. Silicon-based lithium ion battery systems: State-of-the-art from half and full cell viewpoint. *Adv. Funct. Mater.* **2021**, *31*, 2102546.
[41] Han, L.; Liu, T. F.; Sheng, O. W.; Liu, Y. J.; Wang, Y.; Nai, J. W.; Zhang, L.; Tao, X. Y. Undervalued roles of binder in modulating solid electrolyte interphase formation of silicon-based anode materials. *ACS Appl. Mater. Interfaces* **2021**, *13*, 45139–45148.
[42] He, S. G.; Huang, S. M.; Wang, S. F.; Mizota, I.; Liu, X.; Hou, X. H. Considering critical factors of silicon/graphite anode materials for practical high-energy lithium-ion battery applications. *Energy Fuels* **2021**, *35*, 944–964.
[43] Yi, R.; Gordin, M. L.; Wang, D. Integrating Si nanoscale building blocks into micro-sized materials to enable practical applications in lithium-ion batteries. *Nanoscale* **2016**, *8*, 1834–1848.
[44] Zhu, G. J.; Chao, D. L.; Xu, W. L.; Wu, M. H.; Zhang, H. J. Microscale silicon-based anodes: Fundamental understanding and industrial prospects for practical high-energy lithium-ion batteries. *ACS Nano* **2021**, *15*, 15567–15593.
[45] Bourderau, S.; Brousse, T.; Schleich, D. M. Amorphous silicon as a possible anode material for Li-ion batteries. *J. Power Sources* **1999**, *81–82*, 233–236.
[46] Park, C. M.; Kim, J. H.; Kim, H.; Sohn, H. J. Li-alloy based anode materials for Li secondary batteries. *Chem. Soc. Rev.* **2010**, *39*, 3115–3141.
[47] Kim, M.; Yang, Z. Z. Bloom, I. Review-the lithiation/delithiation behavior of Si-based electrodes: A connection between electrochemistry and mechanics. *J. Electrochem. Soc.* **2021**, *168*, 010523.
[48] Feng, Z. Y.; Peng, W. J.; Wang, Z. X.; Guo, H. J.; Li, X. H.; Yan, G. C.; Wang, J. X. Review of silicon-based alloys for lithium-ion battery anodes. *Int. J. Miner. Metall. Mater.* **2021**, *28*, 1549–1564.
[49] Xie, Q. X.; Qu, S. P.; Zhao, P. A facile fabrication of micro/nano-sized silicon/carbon composite with a honeycomb structure as high-stability anodes for lithium-ion batteries. *J. Electroanal. Chem.* **2021**, *884*, 115074.
[50] Zhang, P. J.; Wang, L. B.; Xie, J.; Su, L. W.; Ma, C. A. Micro/nano-complex-structure SiO_x-PANI-Ag composites with homogeneously-embedded Si nanocrystals and nanopores as high-performance anodes for lithium ion batteries. *J. Mater. Chem. A* **2014**, *2*, 3776–3782.
[51] Feng, X. J.; Cui, H. M.; Miao, R. R.; Yan, N. F.; Ding, T. D.; Xiao, Z. Q. Nano/micro-structured silicon@carbon composite with buffer void as anode material for lithium ion battery. *Ceram. Int.* **2016**, *42*, 589–597.
[52] Nzabahimana, J.; Chang, P.; Hu, X. L. Porous carbon-coated ball-milled silicon as high-performance anodes for lithium-ion batteries. *J. Mater. Sci.* **2019**, *54*, 4798–4810.
[53] Park, B. H.; Jeong, J. H.; Lee, G. W.; Kim, Y. H.; Roh, K. C.; Kim, K. B. Highly conductive carbon nanotube micro-spherical network for high-rate silicon anode. *J. Power Sources* **2018**, *394*, 94–101.
[54] Ma, C. L.; Wang, Z. R.; Zhao, Y.; Li, Y.; Shi, J. A novel raspberry-like yolk-shell structured Si/C micro/nano-spheres as high-performance anode materials for lithium-ion batteries. *J. Alloys Compd.* **2020**, *844*, 156201.

[55] Cao, W. Y.; Han, K.; Chen, M. X.; Ye, H. Q.; Sang, S. B. Particle size optimization enabled high initial coulombic efficiency and cycling stability of micro-sized porous Si anode via AlSi alloy powder etching. *Electrochim. Acta* **2019**, *320*, 134613.
[56] An, W. L.; He, P.; Che, Z. Z.; Xiao, C. M.; Guo, E. M.; Pang, C. L.; He, X. Q.; Ren, J. G.; Yuan, G. H.; Du, N. et al. Scalable synthesis of pore-rich Si/C@C core-shell-structured microspheres for practical long-life lithium-ion battery anodes. *ACS Appl. Mater. Interfaces* **2022**, *14*, 10308–10318.
[57] Dai, F.; Zai, J. T.; Yi, R.; Gordin, M. L.; Sohn, H.; Chen, S. R.; Wang, D. H. Bottom-up synthesis of high surface area mesoporous crystalline silicon and evaluation of its hydrogen evolution performance. *Nat. Commun.* **2014**, *5*, 3605.
[58] Lee, J.; Moon, J.; Han, S. A.; Kim, J.; Malgras, V.; Heo, Y. U.; Kim, H.; Lee, S. M.; Liu, H. K.; Dou, S. X. et al. Everlasting living and breathing gyroid 3D network in Si@SiO_x/C nanoarchitecture for lithium ion battery. *ACS Nano* **2019**, *13*, 9607–9619.
[59] Lee, J. I.; Lee, K. T.; Cho, J.; Kim, J.; Choi, N. S.; Park, S. Chemical-assisted thermal disproportionation of porous silicon monoxide into silicon-based multicomponent systems. *Angew. Chem., Int. Ed.* **2012**, *51*, 2767–2771.
[60] Zhao, T. T.; Zhu, D. L.; Li, W. R.; Li, A. J.; Zhang, J. J. Novel design and synthesis of carbon-coated porous silicon particles as high-performance lithium-ion battery anodes. *J. Power Sources* **2019**, *439*, 227027.
[61] Bang, B. M.; Lee, J. I.; Kim, H.; Cho, J.; Park, S. High-performance macroporous bulk silicon anodes synthesized by template-free chemical etching. *Adv. Energy Mater.* **2012**, *2*, 878–883.
[62] Kim, N.; Park, H.; Yoon, N.; Lee, J. K. Zeolite-templated mesoporous silicon particles for advanced lithium-ion battery anodes. *ACS Nano* **2018**, *12*, 3853–3864.
[63] Zhu, G. J.; Jiang, W., Yang, J. P. Engineering carbon distribution in silicon-based anodes at multiple scales. *Chem. -Eur. J.* **2020**, *26*, 1488–1496.
[64] Tian, H. J.; Tan, X. J.; Xin, F. X.; Wang, C. S.; Han, W. Q. Micro-sized nano-porous Si/C anodes for lithium ion batteries. *Nano Energy* **2015**, *11*, 490–499.
[65] Wang, K.; Pei, S. E.; He, Z. S.; Huang, L. A.; Zhu, S. S.; Guo, J. F.; Shao, H. B.; Wang, J. M. Synthesis of a novel porous silicon microsphere@carbon core-shell composite via *in situ* MOF coating for lithium ion battery anodes. *Chem. Eng. J.* **2019**, *356*, 272–281.
[66] Li, X. L.; Gu, M.; Hu, S. Y.; Kennard, R.; Yan, P. F.; Chen, X. L.; Wang, C. M.; Sailor, M. J.; Zhang, J. G.; Liu, J. Mesoporous silicon sponge as an anti-pulverization structure for high-performance lithium-ion battery anodes. *Nat. Commun.* **2014**, *5*, 4105.
[67] Li, X. L.; Yan, P. F.; Xiao, X. C.; Woo, J. H.; Wang, C. M.; Liu, J.; Zhang, J. G. Design of porous Si/C-graphite electrodes with long cycle stability and controlled swelling. *Energy Environ. Sci.* **2017**, *10*, 1427–1434.
[68] Ren, W. F.; Wang, Y. H.; Zhang, Z. L.; Tan, Q. Q.; Zhong, Z. Y.; Su, F. B. Carbon-coated porous silicon composites as high performance Li-ion battery anode materials: Can the production process be cheaper and greener? *J. Mater. Chem. A* **2016**, *4*, 552–560.
[69] Chen, B. H.; Chuang, S. I.; Duh, J. G. Double-plasma enhanced carbon shield for spatial/interfacial controlled electrodes in lithium ion batteries via micro-sized silicon from wafer waste. *J. Power Sources* **2016**, *331*, 198–207.
[70] Chiu, K. F.; Lai, P. Recycled crystalline micro-sized silicon particles modified by pyrolytic coatings using poly(ether ether ketone) precursor for stable lithium ion battery anodes. *Mater. Sci. Eng. B* **2018**, *228*, 52–59.
[71] Zhang, J. Y.; Zhang, C. Q.; Wu, S. M.; Zheng, J.; Zuo, Y. H.; Xue, C. L.; Li, C. B.; Cheng, B. W. High-performance lithium-ion battery with nano-porous polycrystalline silicon particles as anode. *Electrochim. Acta* **2016**, *208*, 174–179.
[72] Zhou, X. Y.; Chen, S.; Zhou, H. C.; Tang, J. J.; Ren, Y. P.; Bai, T.; Zhang, J. M.; Yang, J. Enhanced lithium ion battery performance of nano/micro-size Si via combination of metal-assisted chemical etching method and ball-milling. *Microporous Mesoporous Mater.* **2018**, *268*, 9–15.
[73] Choi, M. J.; Xiao, Y.; Hwang, J. Y.; Belharouak, I.; Sun, Y. K. Novel strategy to improve the Li-storage performance of micro silicon anodes. *J. Power Sources* **2017**, *348*, 302–310.
[74] Yi, R.; Dai, F.; Gordin, M. L.; Chen, S. R.; Wang, D. H. Micro-sized Si-C composite with interconnected nanoscale building blocks as high-performance anodes for practical application in lithium-ion batteries. *Adv. Energy Mater.* **2013**, *3*, 295–300.
[75] Yi, R.; Dai, F.; Gordin, M. L.; Sohn, H.; Wang, D. H. Influence of silicon nanoscale building blocks size and carbon coating on the performance of micro-sized Si-C composite Li-ion anodes. *Adv. Energy Mater.* **2013**, *3*, 1507–1515.
[76] Yi, R.; Zai, J. T.; D, F.; Gordin, M. L.; Wang, D. H. Dual conductive network-enabled graphene/Si–C composite anode with high areal capacity for lithium-ion batteries. *Nano Energy* **2014**, *6*, 211–218.
[77] Li, B.; Xiao, Z. J.; Zai, J. T.; Chen, M.; Wang, H. H.; Liu, X. J.; Li, G.; Qian, X. F. A candidate strategy to achieve high initial Coulombic efficiency and long cycle life of Si anode materials: Exterior carbon coating on porous Si microparticles. *Mater. Today Energy* **2017**, *5*, 299–304.
[78] Zhang, Y.; Zhang, R.; Chen, S. C.; Gao, H. P.; Li, M. Q.; Song, X. L.; Xin, H. L.; Chen, Z. Diatomite-derived hierarchical porous crystalline-amorphous network for high-performance and sustainable Si anodes. *Adv. Funct. Mater.* **2020**, *30*, 2005956.
[79] An, W. L.; Gao, B.; Mei, S. X.; Xiang, B.; Fu, J. J.; Wang, L.; Zhang, Q. B.; Chu, P. K.; Huo, K. F. Scalable synthesis of ant-nest-like bulk porous silicon for high-performance lithium-ion battery anodes. *Nat. Commun.* **2019**, *10*, 1447.
[80] An, Y. L.; Fei, H. L.; Zeng, G. F.; Ci, L.; Xiong, S. L.; Feng, J. K.; Qian, Y. T. Green, scalable, and controllable fabrication of nanoporous silicon from commercial alloy precursors for high-energy lithium-ion batteries. *ACS Nano* **2018**, *12*, 4993–5002.
[81] Sohn, M.; Lee, D. G.; Park, H. I.; Park, C.; Choi, J. H.; Kim, H. Microstructure controlled porous silicon particles as a high capacity lithium storage material via dual step pore engineering. *Adv. Funct. Mater.* **2018**, *28*, 1800855.
[82] Cao, W. Y.; Chen, M. X.; Liu, Y. F.; Han, K.; Chen, X. F.; Ye, H. Q.; Sang, S. B. $C_2H_2O_4$ etching of AlSi alloy powder: An efficient and mild preparation approach for high performance micro Si anode. *Electrochim. Acta* **2019**, *320*, 134615.
[83] He, W.; Tian, H. J.; Xin, F. X.; Han, W. Q. Scalable fabrication of micro-sized bulk porous Si from Fe-Si alloy as a high performance anode for lithium-ion batteries. *J. Mater. Chem. A* **2015**, *3*, 17956–17962.
[84] Wang, J. Y.; Huang, W.; Kim, Y. S.; Jeong, Y. K.; Kim, S. C.; Heo, J.; Lee, H. K.; Liu, B. F.; Nah, J.; Cui, Y. Scalable synthesis of nanoporous silicon microparticles for highly cyclable lithium-ion batteries. *Nano Res.* **2020**, *13*, 1558–1563.
[85] Tao, Y.; Tian, Y.; An, Y. L.; Wei, C. L.; Li, Y.; Zhang, Q. K.; Feng, J. K. Green and facile fabrication of nanoporous silicon@carbon from commercial alloy with high graphitization degree for high-energy lithium-ion batteries. *Sustainable Mater. Technol.* **2021**, *27*, e00238.
[86] Lv, Y. Y.; Shang, M. W.; Chen, X.; Nezhad, P. S.; Niu, J. J. Largely improved battery performance using a microsized silicon skeleton caged by polypyrrole as anode. *ACS Nano* **2019**, *13*, 12032–12041.
[87] Han, X.; Zhang, Z. Q.; Zheng, G. R.; You, R.; Wang, J. Y.; Li, C.; Chen, S. Y.; Yang, Y. Scalable engineering of bulk porous Si anodes for high initial efficiency and high-areal-capacity lithium-ion batteries. *ACS Appl. Mater. Interfaces* **2019**, *11*, 714–721.
[88] Lu, Z. D.; Liu., N.; Lee, H. W.; Zhao, J.; Li, W. Y.; Li, Y. Z.; Cui, Y. Nonfilling carbon coating of porous silicon micrometer-sized particles for high-performance lithium battery anodes. *ACS Nano* **2015**, *9*, 2540–2547.
[89] Zhang, C. F.; Ma, Q.; Cai, M. Y.; Zhao, Z. Q.; Xie, H. W.; Ning, Z. Q.; Wang, D. H.; Yin, H. Y. Recovery of porous silicon from waste crystalline silicon solar panels for high-performance lithium-ion battery anodes. *Waste Manage.* **2021**, *135*, 182–189.
[90] Ma, J.; Sung, J.; Hong, J.; Chae, S.; Kim, N.; Choi, S. H.; Nam, G.; Son, Y.; Kim, S. Y.; Ko, M. et al. Towards maximized volumetric capacity via pore-coordinated design for large-volume-change lithium-ion battery anodes. *Nat. Commun.* **2019**, *10*, 475.

[91] Yang, X. L.; Zhang, P. C.; Shi, C. C.; Wen, Z. Y. Porous graphite/silicon micro-sphere prepared by *in-situ* carbothermal reduction and spray drying for lithium ion batteries. *ECS Solid State Lett.* **2012**, *1*, M5–M7.
[92] Guan, P.; Zhang, W.; Li, C. Y.; Han, N.; Wang, X. C.; Li, Q. F.; Song, G. J.; Peng, Z.; Li, J. J.; Zhang, L. et al. Low-cost urchin-like silicon-based anode with superior conductivity for lithium storage applications. *J. Colloid. Interface Sci.* **2020**, *575*, 150–157.
[93] Han, J. W.; Kong, D. B.; Lv, W.; Tang, D. M.; Han, D. L.; Zhang, C.; Liu, D. H.; Xiao, Z. C.; Zhang, X. H.; Xiao, J. et al. Caging tin oxide in three-dimensional graphene networks for superior volumetric lithium storage. *Nat. Commun.* **2018**, *9*, 402.
[94] Gauthier, M.; Mazouzi, D.; Reyter, D.; Lestriez, B.; Moreau, P.; Guyomard, Do.; Roué, L. A low-cost and high performance ball-milled Si-based negative electrode for high-energy Li-ion batteries. *Energy Environ. Sci.* **2013**, *6*, 2145–2155.
[95] Yang, Y. X.; Qu, X. L.; Zhang, L. C.; Gao, M. X.; Liu, Y. F.; Pan, H. G. Reaction-ball-milling-driven surface coating strategy to suppress pulverization of microparticle Si anodes. *ACS Appl. Mater. Interfaces* **2018**, *10*, 20591–20598.
[96] Li, C.; Ju, Y. H.; Qi, L.; Yoshitake, H.; Wang, H. Y. A micro-sized Si-CNT anode for practical application via a one-step, low-cost and green method. *RSC Adv.* **2017**, *7*, 54844–54851.
[97] Loveridge, M. J.; Lain, M. J.; Huang, Q. Y.; Wan, C. Y.; Roberts, A. J.; Pappas, G. S.; Bhagat, R. Enhancing cycling durability of Li-ion batteries with hierarchical structured silicon-graphene hybrid anodes. *Phys. Chem. Chem. Phys.* **2016**, *18*, 30677–30685.
[98] Liu, X. X.; Chao, D. L.; Zhang, Q.; Liu, H.; Hu, H. L.; Zhao, J. P.; Li, Y.; Huang, Y. Z.; Lin, J. Y.; Shen, Z. X. The roles of lithium-philic giant nitrogen-doped graphene in protecting micron-sized silicon anode from fading. *Sci. Rep*. **2015**, *5*, 15665.
[99] Kang, M. S.; Heo, I.; Kim, S.; Yang, J.; Kim, J.; Min, S. J.; Chae, J.; Yoo, W. C. High-areal-capacity of micron-sized silicon anodes in lithium-ion batteries by using wrinkled-multilayered-graphenes. *Energy Stor. Mater.* **2022**, *50*, 234–242.
[100] Li, Y. Z.; Yan, K.; Lee, H. W.; Lu, Z. D.; Liu, N.; Cui, Y. Growth of conformal graphene cages on micrometre-sized silicon particles as stable battery anodes. *Nat. Energy* **2016**, *1*, 15029.
[101] Sung, J.; Ma, J.; Choi, S. H.; Hong, J.; Kim, N.; Chae, S.; Son, Y.; Kim, S. Y.; Cho, J. Fabrication of lamellar nanosphere structure for effective stress-management in large-volume-variation anodes of high-energy lithium-ion batteries. *Adv. Mater.* **2019**, *31*, 1900970.
[102] Wang, J. Y.; Liao, L.; Li, Y. Z.; Zhao, J.; Shi, F. F.; Yan, K.; Pei, A.; Chen, G. X.; Li, G. D.; Lu, Z. Y. et al. Shell-protective secondary silicon nanostructures as pressure-resistant high-volumetric-capacity anodes for lithium-ion batteries. *Nano Lett.* **2018**, *18*, 7060–7065.
[103] Qin, Z.; Jung, G. S.; Kang, M. J.; Buehler, M. J. The mechanics and design of a lightweight three-dimensional graphene assembly. *Sci. Adv.* **2017**, *3*, e1601536.
[104] Zhang, X. H.; Guo, R. Y.; Li, X. L.; Zhi, L. J. Scallop-inspired shell engineering of microparticles for stable and high volumetric capacity battery anodes. *Small* **2018**, *14*, 1800752.
[105] Chen, F. Q.; Han, J. W.; Kong, D. B.; Yuan, Y. F.; Xiao, J.; Wu, S. C.; Tang, D. M.; Deng, Y. Q.; Lv, W.; Lu, J. et al. 1,000 $Wh{\cdot}L^{-1}$ lithium-ion batteries enabled by crosslink-shrunk tough carbon encapsulated silicon microparticle anodes. *Natl. Sci. Rev.* **2021**, *8*, nwab012.
[106] Shen, Q. Y.; Zheng, R. B.; Lv, Y. Y.; Lou, Y. Y.; Shi, L. Y.; Yuan, S. Scalable fabrication of silicon-graphite microsphere by mechanical processing for lithium-ion battery anode with large capacity and high cycling stability. *Batteries Supercaps* **2022**, *5*, e202200186.
[107] Wei, D. H.; Gao, X.; Zeng, S. Y.; Li, H. B.; Li, H. Y; Li, W. Z.; Tao, X. Q.; Xu, L. L.; Chen, P. Improving the performance of micro-silicon anodes in lithium-ion batteries with a functional carbon nanotube interlayer. *ChemElectroChem* **2018**, *5*, 3143–3149.
[108] Ren, Y.; Yin, X. C.; Xiao, R.; Mu, T. S.; Huo, H.; Zuo, P. J.; Ma, Y. L.; Cheng, X. Q; Gao, Y. Z.; Yin, G. P. et al. Layered porous silicon encapsulated in carbon nanotube cage as ultra-stable anode for lithium-ion batteries. *Chem. Eng. J.* **2022**, *431*, 133982.
[109] Feng, X. J.; Ding, T. D.; Cui, H. M.; Yan, N. F.; Wang, F. A low-cost nano/micro structured-silicon-MWCNTs from nano-silica for lithium storage. *Nano* **2016**, *11*, 1650031.
[110] Zhang, Z. Q.; Han, X.; Li, L. C.; Su, P. F.; Huang, W.; Wang, J. Y.; Xu, J. F.; Li, C.; Chen, S. Y.; Yang, Y. Tailoring the interfaces of silicon/carbon nanotube for high rate lithium-ion battery anodes. *J. Power Sources* **2020**, *450*, 227593.
[111] Park, S. H.; King, P. J.; Tian, R. Y.; Boland, C. S.; Coelho, J.; Zhang, C. F.; McBean, P.; McEvoy, N.; Kremer, M. P.; Daly, D. et al. High areal capacity battery electrodes enabled by segregated nanotube networks. *Nat. Energy* **2019**, *4*, 560–567.
[112] Li, G.; Huang, L. B.; Yan, M. Y.; Li, J. Y.; Jiang, K. C.; Yin, Y. X.; Xin, S.; Xu, Q.; Guo, Y. G. An integral interface with dynamically stable evolution on micron-sized SiO_x particle anode. *Nano Energy* **2020**, *74*, 104890.
[113] Yi, Z.; Lin, N.; Zhao, Y. Y.; Wang, W. W; Qian, Y.; Zhu, Y. C.; Qian, Y. T. A flexible micro/nanostructured Si microsphere cross-linked by highly-elastic carbon nanotubes toward enhanced lithium ion battery anodes. *Energy Storage Mater.* **2019**, *17*, 93–100.
[114] Zhang, Z. Y.; Li, Z. W.; Luo, Q.; Yang, B. Z.; Liu, Y.; Hu, Y. Y.; Liu, X. B.; Yin, Y. H.; Li, Y. S.; Wu, Z. P. Spontaneous nanominiaturization of silicon microparticles with structural stability as flexible anodes for lithium ion batteries. *Carbon* **2022**, *188*, 238–245.
[115] Cai, H. Y.; Han, K.; Jiang, H.; Wang, J. W.; Liu, H. Self-standing silicon-carbon nanotube/graphene by a scalable *in situ* approach from low-cost Al-Si alloy powder for lithium ion batteries. *J. Phys. Chem. Solids* **2017**, *109*, 9–17.
[116] Lee, S. J.; Joe, Y. S.; Yeon, J. S.; Min, D. H.; Shin, K. H.; Baek, S. Ha.; Xiong, P. X.; Nakhanivej, P.; Park, H. S. Hierarchically structured silicon/graphene composites wrapped by interconnected carbon nanotube branches for lithium-ion battery anodes. *Int. J. Energy Res.* **2022**, *46*, 15627–15638.
[117] Gao, X. F.; Wang, F. F; Gollon, S.; Yuan, C. Micro silicon-graphene-carbon nanotube anode for full cell lithium-ion battery. *J. Electrochem. Energy Convers. Storage* **2019**, *16*, 011009.
[118] Shin, M. S.; Choi, C. K.; Park, M. S.; Lee, S. M. Spherical silicon/CNT/carbon composite wrapped with graphene as an anode material for lithium-ion batteries. *J. Electrochem. Sci. Technol.* **2022**, *13*, 159–166.
[119] Lyu, F.; Sun, Z. F.; Nan, B.; Yu, S. C.; Cao, L. J.; Yang, M. Y.; Li, M. C.; Wang, W. X.; Wu, S. F.; Zeng, S. S. et al. Low-cost and novel Si-based gel for Li-ion batteries. *ACS Appl. Mater. Interfaces* **2017**, *9*, 10699–10707.
[120] Qu, F. M.; She, G. W.; Wang, J. T.; Qi, X. P.; Li, S. Y.; Zhang, S. Y.; Mu, L. X.; Shi, W. S. Coating nanoparticle-assembled Si microspheres with carbon for anode material in lithium-ion battery. *J. Phys. Chem. Solids* **2019**, *124*, 312–317.
[121] Tao, J.; Wang, F.; Han, F.; He, Y. L.; Zhang, F. Q.; Liu, J. S. Improving the lithium storage performance of micro-sized SiO_x particles by uniform carbon interphase encapsulation and suitable SiO_2 buffer component. *Electrochim. Acta* **2021**, *385*, 138431.
[122] Lee, Y.; Lee, T.; Hong, J.; Sung, J.; Kim, N.; Son, Y.; Ma, J.; Kim, S. Y.; Cho, J. Stress relief principle of micron-sized anodes with large volume variation for practical high-energy lithium-ion batteries. *Adv. Funct. Mater.* **2020**, *30*, 2004841.
[123] Wang, D. S.; Gao, M. X.; Pan, H. G.; Liu, Y. F.; Wang, J. H.; Li, S. Q.; Ge, H. W. Enhanced cycle stability of micro-sized Si/C anode material with low carbon content fabricated via spray drying and *in situ* carbonization. *J. Alloys Compd.* **2014**, *604*, 130–136.
[124] Zhang, C. Q.; Yang, F.; Zhang, D. L.; Zhang, X.; Xue, C. L.; Zuo, Y. H.; Li, C. B.; Cheng, B. W.; Wang, Q. M. A binder-free Si-based anode for Li-ion batteries. *RSC Adv.* **2015**, *5*, 15940–15943.
[125] Shen, C. X.; Fu, R. S.; Guo, H. C.; Wu, Y. K.; Fan, C. Z.; Xia, Y. G.; Liu, Z. P. Scalable synthesis of Si nanowires interconnected SiO_x anode for high performance lithium-ion batteries. *J. Alloys Compd.* **2019**, *783*, 128–135.
[126] Zhou, Y.; Tian, Z. Y.; Fan, R. J.; Zhao, S. R.; Zhou, R.; Guo, H. J.; Wang, Z. X. Scalable synthesis of Si/SiO_2@C composite from micro-silica particles for high performance lithium battery anodes. *Powder Technol.* **2015**, *284*, 365–370.
[127] Mishra, K.; George, K.; Zhou, X. D. Submicron silicon anode

stabilized by single-step carbon and germanium coatings for high capacity lithium-ion batteries. *Carbon* **2018**, *138*, 419–426.
[128] Yang, T. T.; Ying, H. J.; Zhang, S. L.; Wang, J. L.; Zhang, Z.; Han, W. Q. Electrochemical performance enhancement of micro-sized porous Si by integrating with nano-Sn and carbonaceous materials. *Materials* **2021**, *14*, 920.
[129] Liu, C.; Xia, Q.; Liao, C.; Wu, S. P. Pseudocapacitance contribution to three-dimensional micro-sized silicon@Fe_3O_4@few-layered graphene for high-rate and long-life lithium ion batteries. *Mater. Today Commun.* **2019**, *18*, 66–73.
[130] Li, S. F.; Huang, J. H.; Wang, J.; Han, K. Micro-sized porous silicon@PEDOT with high rate capacity and stability for Li-ion battery anode. *Mater. Lett.* **2021**, *293*, 129712.
[131] Huang, S. Q.; Cheong, L. Z.; Wang, D. Y.; Shen, C. Nanostructured phosphorus doped silicon/graphite composite as anode for high-performance lithium-ion batteries. *ACS Appl. Mater. Interfaces* **2017**, *9*, 23672–23678.
[132] Kim, S. O.; Manthiram, A. A facile, low-cost synthesis of high-performance silicon-based composite anodes with high tap density for lithium-ion batteries. *J. Mater. Chem. A* **2015**, *3*, 2399–2406.
[133] Yang, Y. X.; Ni, C. L.; Gao, M. X.; Wang, J. W.; Liu, Y. F.; Pan, H. G. Dispersion-strengthened microparticle silicon composite with high anti-pulverization capability for Li-ion batteries. *Energy Storage Mater.* **2018**, *14*, 279–288.
[134] Liao, C.; Wu, S. P. Pseudocapacitance behavior on Fe_3O_4-pillared SiO_x microsphere wrapped by graphene as high performance anodes for lithium-ion batteries. *Chem. Eng. J.* **2019**, *355*, 805–814.
[135] Cheng, X. L.; Hu, M.; Huang, R.; Jiang, J. S. HF-free synthesis of anatase TiO_2 nanosheets with largely exposed and clean {001} facets and their enhanced rate performance as anodes of lithium-ion battery. *ACS Appl. Mater. Interfaces* **2014**, *6*, 19176–19183.
[136] Sun, C. H.; Yang, X. H.; Chen, J. S.; Li, Z.; Lou, X. W.; Li, C. Z.; Smith, S. C.; Lu, G. Q.; Yang, H. G. Higher charge/discharge rates of lithium-ions across engineered TiO_2 surfaces leads to enhanced battery performance. *Chem. Commun.* **2010**, *46*, 6129–6131.
[137] Xiao, Z. X.; Yu, C. H.; Lin, X. Q.; Chen, X.; Zhang, C. X.; Jiang, H. R.; Zhang, R. F.; Wei, F. TiO_2 as a multifunction coating layer to enhance the electrochemical performance of SiO_x@TiO_2@C composite as anode material. *Nano Energy* **2020**, *77*, 105082.
[138] Xia, Q.; Xu, A. D.; Du, L.; Yan, Y. R.; Wu, S. P. High-rate, long-term performance of LTO-pillared silicon/carbon composites for lithium-ion batteries anode under high temperature. *J. Alloys Compd.* **2019**, *800*, 50–57.
[139] Heist, A.; Piper, D. M.; Evans, T.; Kim, S. C.; Han, S. S.; Oh, K. H.; Lee, S. H. Self-contained fragmentation and interfacial stability in crude micron-silicon anodes. *J. Electrochem. Soc.* **2018**, *165*, A244–A250.
[140] Kim, D.; Park, M.; Kim, S. M.; Shim, H. C.; Hyun, S.; Han, S. M. Conversion reaction of nanoporous ZnO for stable electrochemical cycling of binderless Si microparticle composite anode. *ACS Nano* **2018**, *12*, 10903–10913.
[141] Wang, C.; Wu, H.; Chen, Z.; McDowell, M. T.; Cui, Y.; Bao, Z. N. Self-healing chemistry enables the stable operation of silicon microparticle anodes for high-energy lithium-ion batteries. *Nat. Chem.* **2013**, *5*, 1042–1048.
[142] Munaoka, T.; Yan, X. Z.; Lopez, J.; To, J. W. F.; Park, J.; Tok, J. B. H.; Cui, Y.; Bao, Z. N. Ionically conductive self-healing binder for low cost Si microparticles anodes in Li-ion batteries. *Adv. Energy Mater.* **2018**, *8*, 1703138.
[143] Xu, Z. X.; Yang, J.; Zhang, T.; Nuli, Y.; Wang, J. L.; Hirano, S. I. Silicon microparticle anodes with self-healing multiple network binder. *Joule* **2018**, *2*, 950–961.
[144] Deng, L.; Zheng, Y.; Zheng, X. M.; Or, T.; Ma, Q. Y.; Qian, L. T.; Deng, Y. P.; Yu, A. P.; Li, J. T.; Chen, Z. W. Design criteria for silicon-based anode binders in half and full cells. *Adv. Energy Mater.* **2022**, *12*, 2200850.
[145] Choi, S.; Kwon, T. W.; Coskun, A.; Choi, J. W. Highly elastic binders integrating polyrotaxanes for silicon microparticle anodes in lithium ion batteries. *Science* **2017**, *357*, 279–283.
[146] Guan, X.; Yong, Y. X.; Wu, Q. P.; Zhang, X. W.; Guo, X. H.; Li, C. L.; Xu, J. Metal-chelated biomimetic polyelectrolyte as a powerful binder for high-performance micron silicon anodes. *Energy Technol.* **2020**, *8*, 2000278.
[147] Tian, M.; Wu, P. Y. Nature plant polyphenol coating silicon submicroparticle conjugated with polyacrylic acid for achieving a high-performance anode of lithium-ion battery. *ACS Appl. Energy Mater.* **2019**, *2*, 5066–5073.
[148] Yu, Y. Y.; Gao, H. H; Zhu, J. D; Li, D. Z.; Wang, F. X.; Jiang, C. H.; Zhong, T. H. Y.; Liang, S. H.; Jiang, M. J. Ionic/electronic conductivity regulation of n-type polyoxadiazole lithium sulfonate conductive polymer binders for high-performance silicon microparticle anodes. *Chin. Chem. Lett.* **2021**, *32*, 203–209.
[149] Song, Z. B.; Chen, S. M.; Zhao, Y.; Xue, S. D.; Qian, G. Y.; Fang, J. J.; Zhang, T. H.; Long, C. J.; Yang, L. Y.; Pan, F. Constructing a resilient hierarchical conductive network to promote cycling stability of SiO_x anode via binder design. *Small* **2021**, *17*, 2102256.
[150] Song, Z. B.; Zhang, T. H.; Wang, L.; Zhao, Y.; Li, Z. K.; Zhang, M.; Wang, K.; Xue, S. D.; Fang, J. J.; Ji, Y. C. et al. Bio-inspired binder design for a robust conductive network in silicon-based anodes. *Small Methods* **2022**, *6*, 2101591.
[151] Yu, Y. Y.; Zhu, J. D.; Zeng, K.; Jiang, M. J. Mechanically robust and superior conductive n-type polymer binders for high-performance micro-silicon anodes in lithium-ion batteries. *J. Mater. Chem. A* **2021**, *9*, 3472–3481.
[152] Woo, H.; Gil, B.; Kim, J.; Park, K.; Yun, A. J.; Kim, J.; Nam, S.; Park, B. Metal-coordination mediated polyacrylate for high performance silicon microparticle anode. *Batteries Supercaps* **2020**, *3*, 1287–1295.
[153] Hu, Y. Y.; You, J. H.; Zhang, S. J.; Lin, H.; Ren, W. F.; Deng, L.; Pan, S. Y.; Huang, L.; Zhou, Y.; Li, J. T. et al. $Li_{0.5}$PAA domains filled in porous sodium alginate skeleton: A 3D bicontinuous composite network binder to stabilize micro-silicon anode for high-performance lithium ion battery. *Electrochim. Acta* **2021**, *386*, 138361.
[154] Huang, L. H.; Chen, D.; Li, C. C.; Chang, Y. L.; Lee, J. T. Dispersion homogeneity and electrochemical performance of Si anodes with the addition of various water-based binders. *J. Electrochem. Soc.* **2018**, *165*, A2239–A2246.
[155] Lopez, J.; Chen, Z.; Wang, C.; Andrews, S. C.; Cui, Y.; Bao, Z. N. The effects of cross-linking in a supramolecular binder on cycle life in silicon microparticle anodes. *ACS Appl. Mater. Interfaces* **2016**, *8*, 2318–2324.
[156] Luo, C.; Du, L. L.; Wu, W.; Xu, H. L; Zhang, G. Z.; Li, S.; Wang, C. Y.; Lu, Z. G.; Deng, Y. H. Novel lignin-derived water-soluble binder for micro silicon anode in lithium-ion batteries. *ACS Sustainable Chem. Eng.* **2018**, *6*, 12621–12629.
[157] Ma, L.; Niu, S. L.; Zhao, F. F.; Tang, R. X.; Zhang, Y.; Su, W. D.; Wei, L. M.; Tang, G.; Wang, Y.; Pang, A. M. et al. A high-performance polyurethane-polydopamine polymeric binder for silicon microparticle anodes in lithium-ion batteries. *ACS Appl. Energy Mater.* **2022**, *5*, 7571–7581.
[158] Ren, W. F.; Le, J. B.; Li, J. T.; Hu, Y. Y.; Pan, S. Y.; Deng, L.; Zhou, Y.; Huang, L.; Sun, S. G. Improving the electrochemical property of silicon anodes through hydrogen-bonding cross-linked thiourea-based polymeric binders. *ACS Appl. Mater. Interfaces* **2021**, *13*, 639–649.
[159] Wu, H.; Du, N.; Zhang, H.; Yang, D. Voltage-controlled synthesis of Cu-Li_2O@Si core-shell nanorod arrays as high-performance anodes for lithium-ion batteries. *J. Mater. Chem. A* **2014**, *2*, 20510–20514.
[160] Wang, B.; Li, X. L.; Luo, B.; Zhang, X. F.; Shang, Y. Y.; Cao, A. Y.; Zhi, L. J. Intertwined network of Si/C nanocables and carbon nanotubes as lithium-ion battery anodes. *ACS Appl. Mater. Interfaces* **2013**, *5*, 6467–6472.
[161] Philippe, B.; Dedryvère, R.; Gorgoi, M.; Rensmo, H.; Gonbeau, D.; Edström, K. Improved performances of nanosilicon electrodes using the salt LiFSI: A photoelectron spectroscopy study. *J. Am. Chem. Soc.* **2013**, *135*, 9829–9842.

[162] Chen, L. B.; Wang, K.; Xie, X. H.; Xie, J. Y. Effect of vinylene carbonate (VC) as electrolyte additive on electrochemical performance of Si film anode for lithium ion batteries. *J. Power Sources* **2007**, *174*, 538–543.
[163] Chang, Z. H.; Li, X.; Yun, F. L.; Shao, Z. C.; Wu, Z. H.; Wang, J. T.; Lu, S. G. Effect of dual-salt concentrated electrolytes on the electrochemical performance of silicon nanoparticles. *ChemElectroChem* **2020**, *7*, 1135–1141.
[164] Chang, Z. H.; Wang, J. T.; Wu, Z. H.; Gao, M.; Wu, S. J.; Lu, S. G. The electrochemical performance of silicon nanoparticles in concentrated electrolyte. *ChemSusChem* **2018**, *11*, 1787–1796.
[165] Zeng, G. F.; An, Y. L.; Xiong, S. L.; Feng, J. K. Nonflammable fluorinated carbonate electrolyte with high salt-to-solvent ratios enables stable silicon-based anode for next-generation lithium-ion batteries. *ACS Appl. Mater. Interfaces* **2019**, *11*, 23229–23235.
[166] Jia, H. P.; Zou, L. F.; Gao, P. Y.; Cao, X.; Zhao, W. G.; He, Y.; Engelhard, M. H.; Burton, S. D.; Wang, H.; Ren, X. D. et al. High-performance silicon anodes enabled by nonflammable localized high-concentration electrolytes. *Adv. Energy Mater.* **2019**, *9*, 1900784.
[167] Chen, J.; Fan, X. L.; Li, Q.; Yang, H. B; Khoshi, M. R.; Xu, Y. B.; Hwang, S.; Chen, L.; Ji, X.; Yang, C. Y. et al. Electrolyte design for LiF-rich solid-electrolyte interfaces to enable high-performance microsized alloy anodes for batteries. *Nat. Energy* **2020**, *5*, 386–397.
[168] Hou, L. P.; Zhang, X. Q.; Li, B. Q.; Zhang, Q. Cycling a lithium metal anode at 90 °C in a liquid electrolyte. *Angew. Chem., Int. Ed.* **2020**, *59*, 15109–15113.
[169] Rodrigues, M. T. F.; Babu, G.; Gullapalli, H.; Kalaga, K.; Sayed, F. N.; Kato, K.; Joyner, J.; Ajayan, P. M. A materials perspective on Li-ion batteries at extreme temperatures. *Nat. Energy* **2017**, *2*, 17108.
[170] Liu, H. Q.; Wei, Z. B.; He, W. D.; Zhao, J. Y. Thermal issues about Li-ion batteries and recent progress in battery thermal management systems: A review. *Energy Convers. Manage.* **2017**, *150*, 304–330.
[171] Cao, Z.; Zheng, X. Y.; Qu, Q. T.; Huang, Y. H.; Zheng, H. H. Electrolyte design enabling a high-safety and high-performance Si anode with a tailored electrode-electrolyte interphase. *Adv. Mater.* **2021**, *33*, 2103178.
[172] Markevich, E.; Salitra, G.; Rosenman, A.; Talyosef, Y.; Aurbach, D.; Garsuch, A. High performance of thick amorphous columnar monolithic film silicon anodes in ionic liquid electrolytes at elevated temperature. *RSC Adv.* **2014**, *4*, 48572–48575.
[173] Kerr, R.; Mazouzi, D.; Eftekharnia, M.; Lestriez, B.; Dupré, N.; Forsyth, M.; Guyomard, D.; Howlett, P. C. High-capacity retention of Si anodes using a mixed lithium/phosphonium bis(fluorosulfonyl)imide ionic liquid electrolyte. *ACS Energy Lett.* **2017**, *2*, 1804–1809.
[174] Campion, C. L.; Li, W. T.; Lucht, B. L. Thermal decomposition of $LiPF_6$-based electrolytes for lithium-ion batteries. *J. Electrochem. Soc.* **2005**, *152*, A2327–A2334.
[175] Wang, Q. S.; Sun, J. H.; Yao, X. L.; Chen, C. H. Thermal behavior of lithiated graphite with electrolyte in lithium-ion batteries. *J. Electrochem. Soc.* **2006**, *153*, A329–A333.
[176] Liu, Q.; Meng, T.; Yu, L.; Guo, S. T.; Hu, Y. H.; Liu, Z. F.; Hu, X. L. Interface engineering to boost thermal safety of microsized silicon anodes in lithium-ion batteries. *Small Methods* **2022**, 6, 2200380.
[177] Guo, Y.; Wu, S. C.; He, Y. B.; Kang, F. Y.; Chen, L. Q.; Li, H.; Yang, Q. H. Solid-state lithium batteries: Safety and prospects. *eScience* **2022**, *2*, 138–163.
[178] Wu, Y. J.; Wang, S.; Li, H.; Chen, L. Q.; Wu, F. Progress in thermal stability of all-solid-state-Li-ion-batteries. *InfoMat* **2021**, *3*, 827–853.
[179] Huang, Q. Q.; Song, J. X.; Gao, Y.; Wang, D. W.; Liu, S.; Peng, S. F.; Usher, C.; Goliaszewski, A.; Wang, D. H. Supremely elastic gel polymer electrolyte enables a reliable electrode structure for silicon-based anodes. *Nat. Commun.* **2019**, *10*, 5586.
[180] Cho, Y. G.; Park, H.; Lee, J. I.; Hwang, C.; Jeon, Y.; Park, S.; Song, H. K. Organogel electrolyte for high-loading silicon batteries. *J. Mater. Chem. A* **2016**, *4*, 8005–8009.
[181] Tan, D. H. S.; Chen, Y. T.; Yang, H. D.; Bao, W.; Sreenarayanan, B.; Doux, J. M.; Li, W. K.; Lu, B. Y.; Ham, S. Y.; Sayahpour, B. et al. Carbon-free high-loading silicon anodes enabled by sulfide solid electrolytes. *Science* **2021**, *373*, 1494–1499.
[182] Chae, S.; Ko, M.; Kim, K.; Ahn, K.; Cho, J. Confronting issues of the practical implementation of Si anode in high-energy lithium-ion batteries. *Joule* **2017**, *1*, 47–60.
[183] Fu, L. L.; Xu, A. D.; Song, Y.; Ju, J. H.; Sun, H.; Yan, Y. R.; Wu, S. P. Pinecone-like silicon@carbon microspheres covered by Al_2O_3 nano-petals for lithium-ion battery anode under high temperature. *Electrochim. Acta* **2021**, *387*, 138461.
[184] Jung, C. H.; Kim, K. H.; Hong, S. H. An *in situ* formed graphene oxide-polyacrylic acid composite cage on silicon microparticles for lithium ion batteries via an esterification reaction. *J. Mater. Chem. A* **2019**, *7*, 12763–12772.

Qing Liu is currently a PhD candidate in School of Material Science and Engineering, Huazhong University of Science and Technology (HUST) under the supervision of Prof. Xianluo Hu. Her research focuses on high-safety Si-based lithium-ion batteries.

Xianluo Hu is a full professor in School of Materials Science and Engineering at Huazhong University of Science and Technology (HUST). He received his PhD from the Chinese University of Hong Kong (CUHK) in 2007 and subsequently worked as a Postdoctoral Researcher in CUHK and a JSPS Postdoctoral Fellow in National Institute of Materials Science (NIMS) of Japan from 2007 to 2009. His current research interest focuses on safe lithium batteries under extreme conditions.